Imperial College London
Department of Theoretical Physics

The Quantum Backflow Effect

Alec Owens

Submitted in partial fulfilment of the requirements for the degree of Master of Science of Imperial College London

September 20, 2012

Abstract

The quantum phenomenon of probability backflow is explored. This remarkable effect arises when considering the motion of a free particle in one dimension. For a state consisting only of positive momenta, it is possible for probability to flow in the opposite direction to the particle's momentum. A comprehensive review of the literature and some new material is presented on the backflow effect, a subject which has implications for the foundations of quantum theory.

Acknowledgements

I would like to thank my supervisor, Jonathan Halliwell for introducing me to the subject of backflow. It has been a fascinating and thoroughly enjoyable journey which would not have been possible without his continued guidance and support.

In addition I am grateful to James Yearsley for his unfaltering patience in helping me with the computer programme Mathematica. Only now do I fully appreciate the love/hate relationship he spoke about in our first meeting.

My thanks also go to Emilio Pisanty for the initial idea and many useful conversations that led to the material presented in Section(6.4). I hope that it can contribute in some way to the future of the subject.

Contents

1 Introduction

The backflow effect is a remarkable yet relatively unknown phenomenon that occurs in quantum mechanics. It is the source of the following puzzle: For a non-relativistic free particle described by a wave function localized in $x < 0$ and containing only positive momenta, the probability of remaining in $x < 0$ can actually increase with time. Probability flows "backwards" in opposition to momentum in certain regions of the x-axis. A striking illustration of backflow is shown in Fig.(1.1).

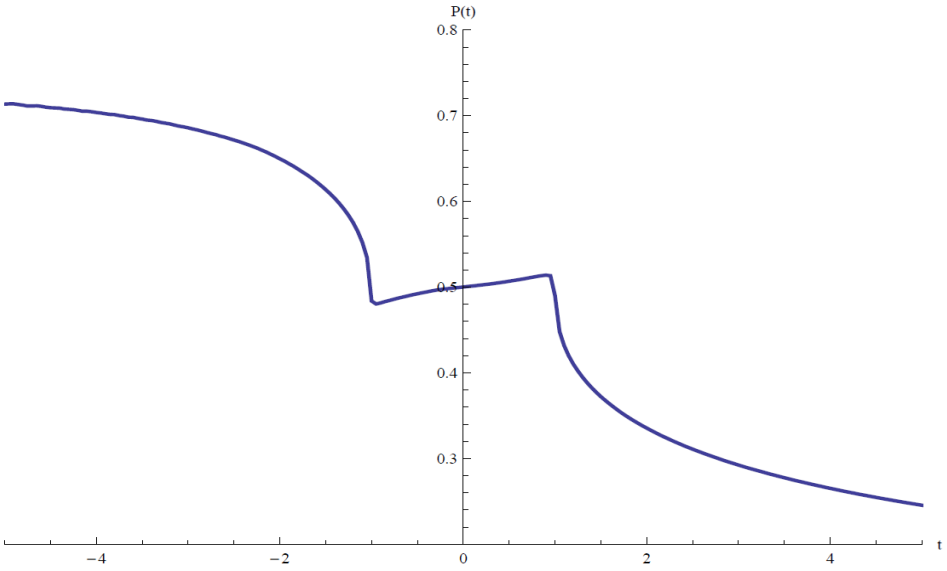

Figure 1.1: Plot of the probability $P(t)$ for remaining in $x < 0$ as a function of time. There is a clear increase in probability during the time interval $[-1, 1]$ [1].

Allcock [2] was the first to identify this effect within the context of the time-of-arrival problem in quantum mechanics. He found that the current $J(x, t)$, can be negative at the origin even for states made up entirely of positive momentum. The occurrence of backflow meant the use of $J(x, t)$ as an ideal arrival time distribution was thus invalid.

Surprisingly, it took over twenty years for a more detailed account of the properties of backflow to emerge. Bracken and Melloy [3] showed that although a period of backflow can be arbitrarily long, the increase in probability for remaining in $x < 0$ can not exceed a certain amount. That is to say, there exists a limit on the total amount of backflow a state can display. This upper bound is given by a dimensionless number c_{bm}, computed numerically to be approximately 0.04. The quantity c_{bm} is independent not only of the mass of the particle but the duration of the time interval over which backflow occurs. It is also independent from $\hbar$ and so one may ask how this strictly quantum effect ceases to exist in classical systems. It is often assumed that letting $\hbar \to 0$ restores the classical limit.

This has led c_{bm} to be dubbed a "new quantum number". However, there are situations where the maximum amount of backflow a state can display becomes dependent on certain physical parameters. Yearsley et al [1] found that the more realistic measurement model of quasiprojectors recovers the naive classical limit and backflow diminishes when $\hbar \to 0$. Furthermore in the relativistic case for particles governed by the Dirac equation [4], c_{bm} has an added dependency on the speed of light c. It has been speculated that particles might literally for some time intervals masquerade as antiparticles during periods of backflow [5]. Equally astounding is that backflow can occur in opposition to a constant force [6].

The numerical computation of c_{bm} has been carried out by a number of authors, most notably by Eveson et al [7], who improved the accuracy to 0.038452. The method they employ is similar to that of Bracken and Melloy, who convert the constant c_{bm} into the supremum of the spectrum of an integral flux operator in momentum space. A more computationally efficient way of finding c_{bm} was put forward by Penz et al [8]. Their approach relied on decomposing the integral operator into a sum of Fourier transformed multiplication operators and then applying the fast Fourier transform. Using linear algebra and functional analysis, they also demonstrated that the flux operator is linear bounded, self-adjoint and not compact.

Another significant result by Penz et al [8] was the numerical calculation of the backflow maximising state and its current. This state produces the greatest amount of backflow but to date, the analytic form is unknown and a vital part of our understanding is missing. Yearsley et al [1] proposed two candidate analytic expressions that appeared to match the numerical solutions of Penz et al. Closer inspection revealed that these states did not exhibit the maximum amount of backflow, however one candidate state displayed around 70% of the theoretical maximum, significantly larger than any previous analytic state discovered.

An interesting set of questions concerns the kind of states which produce backflow and the amount they display in comparison to the backflow maximising state. One can then begin to address the problem of measuring the effect since it has never been observed experimentally. Negative values of the Wigner function of a state give a good indication of non-classical behaviour. However, this is not sufficient and calculations of the probability current and flux are required to demonstrate the occurrence of backflow. A single Gaussian wavepacket will never exhibit backflow but a superposition of two Gaussians will [1]. This is promising as a state of this kind is experimentally viable, but as it only displays around 16% of the theoretical maximum, measuring the effect may prove challenging.

There exist both direct and indirect methods to experimentally realise backflow but this is an area that requires further work. Difficulties arise when considering how to measure the small fraction of backflowing probability. At asymptotic distances from the source or interaction region, the effect of backflow is negligible [9]. This is why the use of time of flight techniques in experiments with atomic and molecular beams is not problematic. If the detectors were moved closer to the interaction region however, non-classical results may become more apparent. Already it has been shown that the backflow effect has surprising implications when considering the concept of perfect absorption in quantum mechanics. During a period of backflow it is possible for a perfect absorber to emit probability [10]. Backflow has also highlighted inconsistencies between

two potential arrival time densities [11].

Recently, backflow has been shown to occur for an electron in a magnetic field [12]. If the wavepacket is made up entirely of states with negative values of the angular momentum quantum number, then there are regions of space where the effective angular momentum is positive and the probability current J is negative. These regions of backflow can be sustained indefinitely for certain wave functions due to the unusual relationship between energy and the angular momentum quantum number.

A period of backflow can be arbitrarily long but ultimately, there is a temporal constraint on the effect specified through the dimensionless quantity c_{bm}. Naturally one may then ask about the spatial extent of backflow. Does there exist a restriction on the regions of the x-axis over which the effect takes place? The work of Eveson et al [7] derived a "kinematical" quantum inequality for the current density demonstrating that backflow is restricted in space. Furthermore, it is possible to give a quantitative measure of the backflowing fraction of the x-axis. This was achieved by Berry [5], who focused on the distribution and evolution of the regions of the x-axis over which backflow occurs. His results indicate that a region of backflow is dependent on the distribution of the component momenta in the wavepacket. In superpositions of many-waves, the region of backflow is much larger when its Fourier components are strongly correlated than if they were randomly distributed, and the state exhibits "strong backflow". This effect, (which is closely related to another quantum phenomenon, superoscillations), is short lived however, as evolution of the state according to the Schrödinger equation causes the destruction of the phases responsible for strong backflow. The region of backflow shrinks and becomes comparable in size to that of a random superposition.

To illustrate the backflow effect, Bracken and Melloy [3] presented a simple description using negative probability, a topic many regard as unsatisfactory. They noted that a flow of positive probability in the negative x-direction is mathematically equivalent to a flow of negative probability in the positive x-direction. Backflow is thus explained by a (net) flow of negative probability in the direction of the particle's momentum. This interpretation is controversial, and backflow is best understood as arising from interference between different parts of the wavepacket. In open system models these interference effects are suppressed by the presence of an environment [13] and backflow ceases to occur. The process of decoherence is a central idea in the emergence of classical behaviour and sheds light on the disappearance of backflow in the standard approach to the classical limit.

Within the framework of Bohmian mechanics an alternative understanding of the backflow effect emerges. Here, the point particle and the matter wave are both regarded as real and distinct physical entities. A particle is not truly free but follows a well defined trajectory, its motion governed by an associated pilot wave. These trajectories do not intersect each other, so only a single trajectory contributes to the probability current $J(x,t)$ at each point in spacetime. When the current at the origin, $J(0,t) > 0$, a particle is crossing $x = 0$ only from the left, whereas any time interval when $J(0,t) < 0$, corresponds to crossing $x = 0$ from the right. Backflow can occur in several disjoint time intervals and so one must accept the counterintuitive property that a free particle can in fact turn back on itself. This does not seem wholly settling, however, in Bohm's theory a particle is always guided by the wave function which itself is susceptible to temporal change in the backflow regions [10].

Probability backflow has also been studied within the decoherent histories approach to quantum mechanics [14, 15]. This formulation applies to genuinely closed quantum systems with the objective being to assign probabilities to coarse grained histories of a quantum system. A history is represented by a time-ordered string of projections together with an initial state. Probabilities can only be assigned if the histories satisfy certain consistency conditions, in particular sets of histories must satisfy the condition of decoherence. For states that display significant backflow, there cannot be decoherence and it is not possible to assign probabilities. This insight is useful in the context of the arrival time problem [16].

Time observables have a much debated history within quantum theory. Unlike other observables such as the position or momentum of a particle, time cannot be represented by a self-adjoint operator. Instead, it enters the Schrödinger equation as an external parameter t. Probability backflow together with the Zeno effect [17], provide a fundamental limitation on the accuracy with which we can define time observables. A better understanding of the backflow effect could give useful insight into the definition of time observables, an issue central to the foundations of quantum theory.

Despite its discovery over forty years ago, there is only a small amount of literature on the subject of backflow. There are still many open questions concerning the experimental observation of the effect and the analytic form of the backflow maximising state. The purpose of this report is to provide a comprehensive review of the backflow effect. It is a fascinating subject that encapsulates the weird and wonderful nature of quantum mechanics and for that reason alone, it deserves further study.

2 The Backflow Effect

2.1 Backflow and the Wigner Function

We consider a free non-relativistic particle described by the normalised wave function $\psi(x,t)$. The wave packet is localised in $x<0$ and consists entirely of positive momenta. The motion is confined to the x-axis (although the arguments can be extended to three dimensions, this would unnecessarily complicate matters).

In terms of ψ, the probability density $\rho(x,t)$ and probability current $J(x,t)$ are defined by

$$\rho(x,t)=\psi^*(x,t)\psi(x,t) \tag{2.1}$$

$$J(x,t)=-\frac{i\hbar}{2m}\left(\psi^*(x,t)\frac{\partial\psi(x,t)}{\partial x}-\frac{\partial\psi^*(x,t)}{\partial x}\psi(x,t)\right) \tag{2.2}$$

and satisfy the continuity equation,

$$\frac{\partial\rho(x,t)}{\partial t}+\frac{\partial J(x,t)}{\partial x}=0 \tag{2.3}$$

The probability for the particle to be in the spatial region $[-\infty,0]$ at time t is

$$P(t)=\int_{-\infty}^{0}\mathrm{d}x\,\rho(x,t) \tag{2.4}$$

and provided that $J(-\infty,t)=0$, it follows that

$$\frac{dP(t)}{dt}=-J(0,t) \tag{2.5}$$

Classically, because $J(0,t)\geq 0$ for all $t>0$, Eq.(2.5) expresses the result expected intuitively; the probability that the particle is in the region $[-\infty,0]$ decreases monotonically with time. However, quantum mechanics permits $J(0,t)<0$ and so $P(t)$ can actually increase with time. This illustrates the backflow effect where probability can flow in the opposite direction to a particle's momentum. The effect can last for an arbitrarily long period of time but there is a limit on how much probability can flow "backwards". We will discuss the characteristics of backflow later on in the chapter.

The negativity of the current is closely related to the Wigner function and it is this relationship that we will now develop to shed some light on this peculiar quantum phenomenon. We consider the amount of probability flux $F(t_1,t_2)$ crossing $x=0$ during the time interval $[t_1,t_2]$, defined by

$$F(t_1,t_2)=\int_{-\infty}^{0}\mathrm{d}x\,\rho(x,t_1)-\int_{-\infty}^{0}\mathrm{d}x\,\rho(x,t_2)$$

$$= \int_{t_1}^{t_2} \mathrm{d}t\, J(0,t) \tag{2.6}$$

where the current can be written in terms of the Wigner function [18], $W(x,p,t)$ at time t,

$$J(0,t) = \int \mathrm{d}p\, \frac{p}{m} W(0,p,t) \tag{2.7}$$

For a free particle, the Wigner function evolves according to,

$$W(x,p,t) = W(x - \frac{pt}{m}, p, 0) \tag{2.8}$$

If we take a time interval $[0,T]$ over which backflow occurs, the flux can now be expressed as

$$F(0,T) = \int_0^T \mathrm{d}t \int \mathrm{d}p\, \frac{p}{m} W(-pt/m, p, 0) \tag{2.9}$$

The Wigner function can be negative due to the effects of quantum interference between different portions of the state. It is this negativity that is a necessary condition for the negativity of the flux (and current [14]). It is not a sufficient condition however, since the integral in Eq.(2.9) may give a positive expression, even for negative values of W.

Feynman [19] argued in favour of negative probabilities as a way to interpret negative values of the Wigner function. Bracken and Melloy [3] then developed this idea to provide a simple picture of backflow. For wave functions where W vanishes for $p < 0$, the current is

$$J(x,t) = \int_0^\infty \mathrm{d}p\, \frac{p}{m} W(x - pt/m, p, 0) \tag{2.10}$$

From this expression we see that all the probability flows in the direction of the particle's momentum. However, not all the probability is positive. A flow of positive probability in the negative x-direction is mathematically equivalent to a flow of negative probability in the positive x-direction. They thus conclude that backflow is explained by a (net) flow of negative probability in the direction of the particle's momentum.

Negative probabilities are a contentious topic that many regard as unsatisfactory. No one can dispute their use as a mathematical tool but how does one interpret them physically? Quantum mechanics has a long history of revealing aspects of nature that go against our classical intuition and backflow is certainly one of them. Regardless of their interpretation, negative probabilities do provide a simple understanding of this quantum effect.

Note that when considering open systems models, evolution in the presence of an environment can cause the Wigner function to become strictly positive after a short time [20]. As a result, the flux will be positive as can be seen from Eq.(2.9). Backflow is destroyed by the presence of an environment. This is expected since it is clearly a non-classical effect which must vanish in the appropriate classical limit. This and other aspects of the classical limit of backflow will be discussed further in Chapter 5.

2.2 Operator Form

We wish to express the flux, Eq.(2.6), in an operator form [1]. This enables us to find the limit on the total amount of backflow that can occur by looking at the spectrum of the flux operator, $\hat{F}(t_1, t_2)$. We introduce a projection operator onto the positive x-axis, $\Pi = \theta(\hat{x})$, and its complement, $\bar{\Pi} = \mathbb{1} - \Pi = \theta(-\hat{x})$. The flux operator is defined by

$$\begin{aligned}\hat{F}(t_1, t_2) &= \Pi(t_2) - \Pi(t_1) \\ &= \int_{t_1}^{t_2} \mathrm{d}t\, \dot{\Pi}(t)\end{aligned} \tag{2.11}$$

and using Heisenberg's equation of motion for $\dot{\Pi}(t)$,

$$\begin{aligned}\hat{F}(t_1, t_2) &= \int_{t_1}^{t_2} \mathrm{d}t\, \frac{i}{\hbar}[H, \theta(\hat{x})] \\ &= \int_{t_1}^{t_2} \mathrm{d}t\, \hat{J}(t)\end{aligned} \tag{2.12}$$

where the current operator,

$$\hat{J} = \frac{1}{2m}(\hat{p}\delta(\hat{x}) + \delta(\hat{x})\hat{p}) \tag{2.13}$$

The flux Eq.(2.6), and current Eq.(2.2), are now defined by

$$\begin{aligned}F(t_1, t_2) &= \langle \hat{F}(t_1, t_2) \rangle \\ &= \int_{t_1}^{t_2} \mathrm{d}t\, \langle \psi | \hat{J}(t) | \psi \rangle\end{aligned} \tag{2.14}$$

and

$$J(t) = \langle \psi | \hat{J}(t) | \psi \rangle \tag{2.15}$$

Note that in Eq.(2.13), $\hat{p}$ and $\delta(\hat{x})$ are non-negative operators on states with positive momentum but as they do not commute, $\hat{J}$ is not a positive operator and therefore does not satisfy the requirement

$$\langle \psi | \hat{J}(t) | \psi \rangle \geq 0 \tag{2.16}$$

Positive operators arise in quantum mechanics when dealing with probabilities, inherently positive quantities. The fact $\hat{J}$ is not one may be a possible reason for the negativity of the flux, Eq.(2.14).

2.3 The Eigenvalue Equation

We turn our attention to the eigenvalue problem

$$\theta(\hat{p})\hat{F}(t_1,t_2)|\Phi\rangle = \lambda|\Phi\rangle \tag{2.17}$$

where the states $|\Phi\rangle$ consist of only positive momenta. An opposite sign convention to previous work [3, 7, 8] is used, so now states which display backflow have $\lambda < 0$. The most negative eigenvalue of the flux operator is the most negative value of the flux, and this provides a limit on the total amount of backflow that can occur for any state. For convenience, the time interval $[t_1, t_2]$ is chosen to be $[-T/2, T/2]$. The eigenvalue equation in momentum space is then

$$\frac{1}{\pi}\int_0^\infty \mathrm{d}q\, \frac{\sin\left[(p^2-q^2)T/4m\hbar\right]}{(p-q)}\Phi(q) = \lambda\Phi(p) \tag{2.18}$$

If we define rescaled variables u and v by $p = 2\sqrt{m\hbar/T}u$ and $q = 2\sqrt{m\hbar/T}v$ then Eq.(2.18) reduces to

$$\frac{1}{\pi}\int_0^\infty \mathrm{d}v\, \frac{\sin(u^2-v^2)}{(u-v)}\phi(v) = \lambda\phi(u) \tag{2.19}$$

where $\phi(u) = (m\hbar/4T)^{1/4}\Phi(p)$ and is dimensionless. The flux now has the form,

$$F(-T/2, T/2) = \frac{1}{\pi}\int_0^\infty \mathrm{d}u \int_0^\infty \mathrm{d}v\, \phi^*(u)\frac{\sin(u^2-v^2)}{(u-v)}\phi(v) \tag{2.20}$$

Since Eq.(2.19) is real, we can assume without loss of generality that the eigenstates $\phi(u)$ are real valued functions. This means the corresponding wave functions in configuration space will possess the symmetry

$$\psi^*(x,t) = \psi(-x,-t) \tag{2.21}$$

Note also that the eigenvalues λ, including in particular $-c_{bm}$(the most negative λ), are dimensionless and lie in the range

$$-c_{bm} \leq \lambda \leq 1 \tag{2.22}$$

where $c_{bm} = 0.038452$. This value was computed numerically using the computer programme *Mathematica*. To date, Eq.(2.19) has not been solved analytically and instead numerical methods must be used.

The independence from $\hbar, m$ and T, of the quantity c_{bm} invites comment. This "quantum number" describes a strictly quantum effect that has no classical counterpart. In the naive classical limit, $\hbar \to 0$, backflow does not disappear as one might expect, prompting the question; why is backflow not observed in classical systems? It should also be noted that the duration of a period of negative current can be arbitrarily long. This is because the total flux over the time interval is bounded from below by $-c_{bm}$, so

$$\int_{-T/2}^{T/2} \mathrm{d}t\, J(t) \geq -c_{bm} \tag{2.23}$$

and a relationship of the form

$$T\, J(\tau) \geq -c_{bm} \tag{2.24}$$

emerges for some time τ in the interval $[-T/2, T/2]$. Conversely, Eq.(2.24) indicates that the current can be arbitrarily negative if only for a sufficiently short time.

The method used here to calculate c_{bm} follows closely that of Bracken and Melloy [3], who gave the first detailed account of probability backflow. Many authors have since gone on to improve the precision of c_{bm}, most notably Penz et al [8]. These authors decompose the integral flux operator into a sum of Fourier transformed multiplication operators and then apply the fast Fourier transform. The benefit of this method is that the flux operator $\hat{F}(t_1, t_2)$ need not be approximated by a finite square matrix, and so calculating c_{bm} requires less computational effort.

2.4 Properties of the Flux Operator

Penz et al [8] used linear algebra and functional analysis to show that the flux operator, $\hat{F}(t_1, t_2)$, was linear bounded, self-adjoint and not compact. In this section we touch upon the key points of their argument but refer the reader to Ref.[8] for a more detailed analysis.

2.4.1 Linear bounded and self-adjoint

Let a particle have the momentum space wave function ϕ and introduce the orthogonal projection, $\mathcal{O} : L^2(\mathbb{R}) \to L^2(\mathbb{R})$, where

$$(\mathcal{O}f)(x) = \begin{cases} f(x) & \text{for } x > 0 \\ 0 & \text{for } x < 0 \end{cases} \tag{2.25}$$

and $L^2(\mathbb{R})$ is the space of square integrable L^2 functions in $\mathbb{R}$.

Since the spectrum of an operator is invariant under unitary transformation, it holds that for any fixed real time $T > 0$,

$$-c_{bm} = \inf \sigma(\mathcal{O} B_T \mathcal{O}) \tag{2.26}$$

where $\sigma(A)$ denotes the spectrum of a linear operator A, and B_T is the backflow operator introduced by Penz et al [8]. This statement is equivalent to saying that the total amount of negative probability flux that can occur is equal to the most negative value of the spectrum of the flux operator, Eq.(2.12). Thus,

$$-c_{bm} = \inf \sigma(\hat{F}) \tag{2.27}$$

and so,

$$\inf \sigma(\mathcal{O}B_T\mathcal{O}) = \inf \sigma(\hat{F}) \tag{2.28}$$

The unitary equivalence between $\mathcal{O}B_T\mathcal{O}$ and $\hat{F}$, confirms that $\hat{F}$ is linear bounded and self-adjoint. The eigenvalues of the flux operator are therefore real.

2.4.2 Non-compact

The spectrum of $\mathcal{O}B_T\mathcal{O}$ does not vary with T and it follows that

$$-1 \in \sigma(\mathcal{O}B_T\mathcal{O}) \tag{2.29}$$

If $\mathcal{O}B_T\mathcal{O}$ (and equivalently $\hat{F}$) were compact, then -1 would be an eigenvalue and

$$\mathcal{O}B_T\mathcal{O}\phi = -\phi \tag{2.30}$$

However, a lemma that exploits the generalized uniqueness theorem [21] shows a contradiction with the above statement. For a compact operator every nonzero spectral value is an eigenvalue. Since this is not true for $\mathcal{O}B_T\mathcal{O}$, it must be non-compact and therefore

$$\sigma(\mathcal{O}B_T\mathcal{O}) \subset [-c_{bm}, 1] \tag{2.31}$$

This statement is equivalent to Eq.(2.22). Since the flux operator is non-compact it is not necessarily diagonalizable.

2.5 The Backflow Maximising State

The backflow maximising state is found by solving the eigenvalue equation Eq.(2.19). As mentioned earlier, Eq.(2.19) has never been solved analytically and this still remains one of the biggest challenges within the subject of backflow. If the analytic form was known this would be a huge step forward in our understanding and could potentially pave the way to experimental observation of the effect. In Chapter 4 we will look at a possible analytic expression for the backflow maximising state.

An approximate eigenstate, $\phi_{max}(u)$, satisfying Eq.(2.19) with eigenvalue $-c_{bm}$ has been calculated using numerical methods [1, 8]. A plot of $\phi_{max}(u)$ in momentum space is displayed in Fig.(2.1) and the corresponding wave function in configuration space is shown in Fig.(2.2).

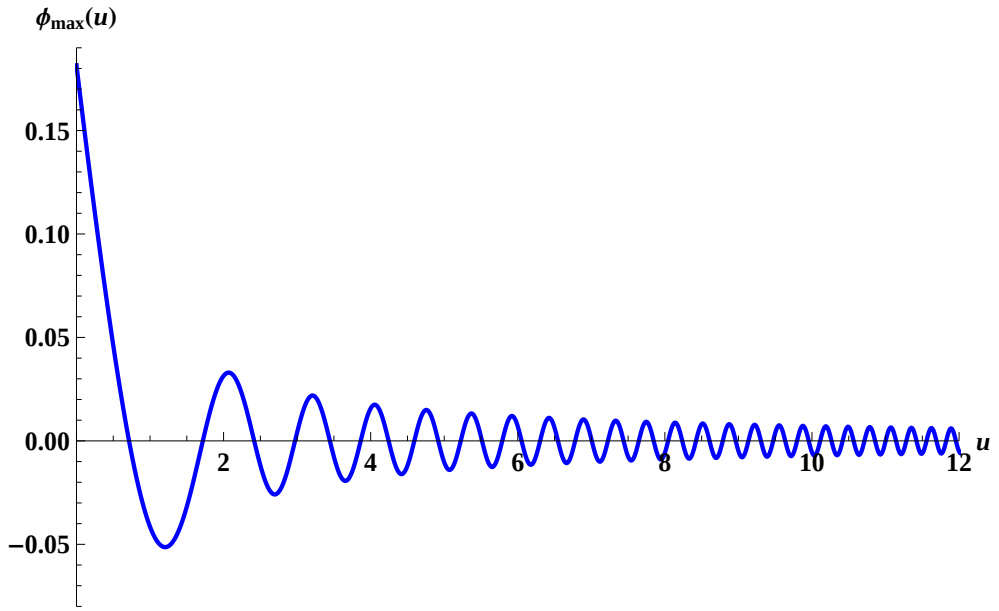

Figure 2.1: Plot of the backflow maximising state, $\phi_{max}(u)$, in momentum space.

Note that in the position representation the wave function at $t = 0$ has even real part and odd imaginary part as alluded to earlier in Eq.(2.21).

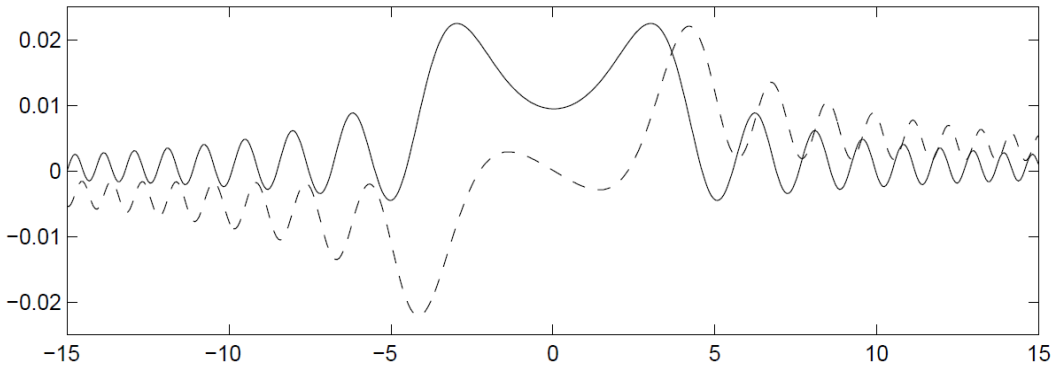

Figure 2.2: Plot of the backflow maximising state in configuration space [8] (real part ——, imaginary part - - -).

The current $J(0, t)$ as a function of time is plotted in Fig.(2.3). The current is negative during the time interval $[-1, 1]$ and appears to be the only period over which $\phi_{max}(u)$ displays backflow. The area below the x-axis and bounded by $J(0, t)$ between $[-1, 1]$ approximately sums up to $-c_{bm}$, as required. There is also a very noticeable singularity structure at $t = \pm 1$ at which the current jumps between $-\infty$ and $+\infty$. This appears to be a distinct signature of the backflow maximising state. Yearsley et al [1] speculate that this is related to some properties of the flux operator. From Eq.(2.12) and Eq.(2.17) it can be seen that the backflow maximising state is an eigenstate of the

current operator $\hat{J}$, and so the state is of the form $\hat{J}|\phi\rangle$ evolved in time. Looking at this quantity may indicate the cause of the jump since the current $J(t) = \langle\phi|\hat{J}|\phi\rangle$.

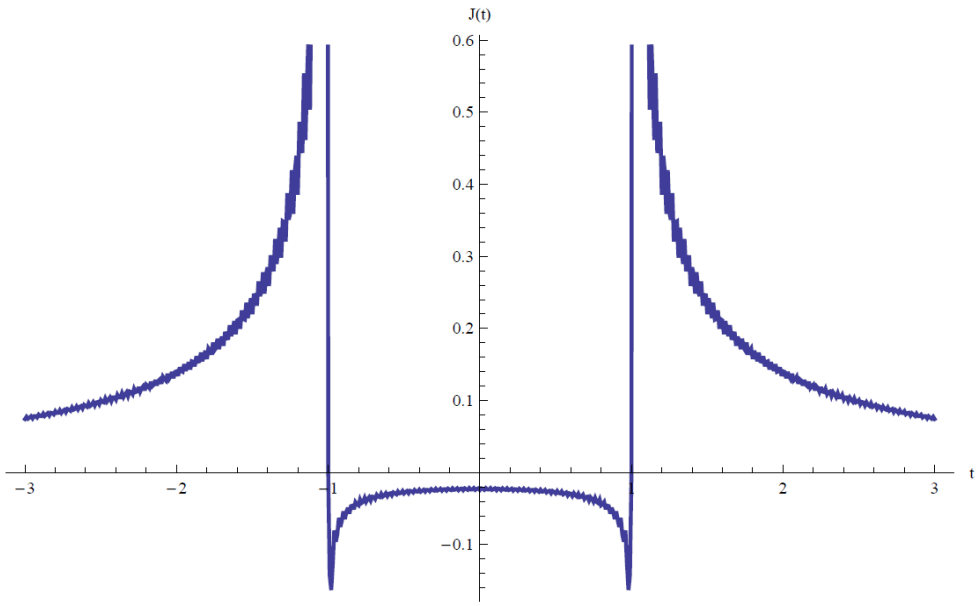

Figure 2.3: Plot of the current $J(0,t)$ for the backflow maximising state $\phi_{max}(u)$ [1].

Penz et al [8] proposed that the state $\phi_{max}(u)$ appears to have the asymptotic form,

$$\phi_{max}(u) \sim \frac{\sin(u^2)}{u} \tag{2.32}$$

If we look at the form $\sin(u^2)/u$, then in terms of the dimensionless parameters u and v, the current at the origin at time $t = 0$ is

$$\begin{aligned} J(0,0) &= \frac{1}{2\pi}\int_0^\infty \mathrm{d}u\,\mathrm{d}v\,(u+v))\phi(u)\phi(v) \\ &= \frac{1}{\pi}\int_0^\infty \mathrm{d}u\,\frac{\sin(u^2)}{u}\int_0^\infty \mathrm{d}v\,\sin(v^2) \\ &= \frac{1}{8}\sqrt{\frac{\pi}{2}} > 0 \end{aligned} \tag{2.33}$$

This value is positive but if we look at Fig.(2.3), the current at $t = 0$ for $\phi_{max}(u)$ is clearly negative. Therefore the backflow maximising state must be very different from $\sin(u^2)/u$ for small u, but may have this form for large u.

3 The Spatial Extent of Backflow

3.1 Introduction

One of the key relationships established in Chapter 2 demonstrated that a period of backflow can be arbitrarily long but ultimately, there is a temporal constraint specified through the dimensionless number c_{bm}. It is natural then to ask about the spatial extent of backflow. Does there exist a restriction on the regions of the x-axis over which the effect takes place?

In this chapter we will show an inequality exists which places a condition on the spatial extent of the negative current. This demonstrates that backflow is limited in space. Furthermore, it is possible to give a quantitative measure of the backflowing fraction of the x-axis. This is an important result that could certainly help in the experimental realisation of backflow. Berry [5] noted that another quantum phenomenon known as superoscillations [22] is closely related to backflow. We will explore this connection, specifically in relation to "strong backflow", an effect that occurs in many-wave superpositions when the component momenta of the wavepacket are strongly correlated.

3.2 Quantum Inequality for the Current

First introduced in quantum field theory, quantum inequalities describe local constraints on the magnitude and duration of negative energy densities. Their significance has been utilised to help understand why the expectation value of an observable density can be arbitrarily negative after quantisation, even though the spatially integrated density is non-negative. The work of Eveson et al [7] focused on the extent to which quantum inequalities may be applied in the context of quantum mechanical systems. Specifically, they derived a "kinematical" quantum inequality for the current density to demonstrate that backflow is limited in space. In this section we review the key steps of their analysis.

As we are looking at the spatial extent of the current at a specific moment in time during a period of backflow, it is convenient to drop the t dependence from our working. We consider a normalised state ψ which is square-integrable and also has a continuous, square-integrable first derivative. It is useful to express the current Eq.(2.2), in the form

$$J(x) = \frac{1}{m}\mathrm{Re}\left(\psi^*(x)\hat{p}\psi(x)\right) \tag{3.1}$$

where $\hat{p}$ is the usual momentum operator, $\hat{p} = -i\hbar\partial/\partial x$. Integrating with respect to x yields,

$$\int \mathrm{d}x\, J(x) = \frac{1}{m}\mathrm{Re}\langle\psi|\hat{p}|\psi\rangle \tag{3.2}$$

By interpreting spatially smeared quantities of the form

$$J(f) = \int \mathrm{d}x\, J(x) f(x) \tag{3.3}$$

as the instantaneous probability current measured by a spatially extended detector, we can write

$$\int \mathrm{d}x\, J(x) f(x) = \frac{1}{m} \mathrm{Re} \langle \psi | \hat{M}_f \hat{p} | \psi \rangle \tag{3.4}$$

where $\hat{M}_f$ is a linear multiplication operator defined by,

$$\hat{M}_f \psi(x) = f(x) \psi(x) \tag{3.5}$$

and $f(x)$ is any smooth, complex-valued function with compact support. Transforming the right hand side of Eq.(3.4) to momentum space gives,

$$\int \mathrm{d}x\, J(x) f(x) = \frac{\hbar}{m} \int \frac{\mathrm{d}p}{2\pi}\, p |\hat{M}_g \phi(p)|^2 \tag{3.6}$$

and if we estimate the portion of the integral on the right hand side of Eq.(3.6) which arises from $p < 0$, a bound emerges

$$\begin{aligned} \int \mathrm{d}x\, J(x) f(x) &\geq \frac{\hbar}{m} \int_{-\infty}^{0} \frac{\mathrm{d}p}{2\pi}\, p |\hat{M}_g \phi(p)|^2 \\ &= -\frac{\hbar}{m} \int_{0}^{\infty} \frac{\mathrm{d}p}{2\pi}\, p |\hat{M}_g \phi(-p)|^2 \end{aligned} \tag{3.7}$$

Utilising the convolution theorem, it holds that

$$\hat{M}_g \phi(p) = \int_0^\infty \frac{\mathrm{d}p'}{2\pi}\, \phi(p') g(p - p'), \qquad p' \in \mathbb{R}^+ \tag{3.8}$$

and because we can choose $g \in C^\infty(\mathbb{R})$ to be real-valued, applying the Cauchy-Schwarz inequality gives,

$$|\hat{M}_g \phi(-p)|^2 \leq \int_0^\infty \frac{\mathrm{d}p'}{2\pi}\, |g(p + p')|^2 \tag{3.9}$$

It is now possible to write Eq.(3.7) as

$$\int \mathrm{d}x\, J(x) f(x) \geq -\frac{\hbar}{m} \int_0^\infty \frac{\mathrm{d}p}{2\pi} \int_0^\infty \frac{\mathrm{d}p'}{2\pi}\, p |g(p + p')|^2 \tag{3.10}$$

and by setting $f(x) = g(x)^2$ and using Parseval's theorem, we arrive at the final result,

$$\int \mathrm{d}x\, J(x) |g(x)|^2 \geq -\frac{\hbar}{8\pi m} \int \mathrm{d}x\, |g'(x)|^2 \tag{3.11}$$

for all normalised states ψ belonging to the class $\mathcal{R}$ of right-moving states defined by

$$\mathcal{R} = \{\psi \in L^2(\mathbb{R}) : \phi(p) = 0 \text{ for } p < 0\} \tag{3.12}$$

As there is no reference to a specific Hamiltonian, this is a kinematical result as oppose to a dynamical one. Note that in the limit $\hbar \to 0$, the inequality disappears. This is in contrast to the result of Bracken and Melloy [3], where the probability $P(t)$ for remaining in $x < 0$ satisfies

$$P(t) \leq P(0) + c_{bm} \tag{3.13}$$

and does not vanish when $\hbar \to 0$, since c_{bm} is dimensionless.

There are two interesting comments to be made on Eq.(3.11). Firstly, there is no upper bound on the smeared current. If we define,

$$\psi_\kappa(x) = e^{i\kappa x}\psi(x) \tag{3.14}$$

for any normalised $\psi \in \mathcal{R}$, then $\psi_\kappa \in \mathcal{R}$ for all $\kappa \geq 0$. The current becomes,

$$J_\kappa(x) = J(x) + \frac{\kappa\hbar}{m}|\psi(x)|^2 \tag{3.15}$$

and it is evident that,

$$\int \mathrm{d}x\, J_\kappa(x)g(x) \to \infty \text{ as } \kappa \to \infty \tag{3.16}$$

The current can be arbitrarily negative. This coincides with the relationship Eq.(2.24), which also established the current can be arbitrarily negative if only for a sufficiently short time.

Secondly, the magnitude of the negative current times the square of its spatial extent is bounded above for all right moving states in $\mathcal{R}$. This can be seen by replacing g with $g_\kappa(x) = \kappa^{1/2} f(x/\kappa)$ in Eq.(3.11), and noting the right hand side of Eq.(3.11) scales by a factor of κ^{-2}. The limit $\kappa \to 0$, corresponds to the fact the current can be arbitrarily negative at a point, while the limit $\kappa \to \infty$ is consistent with $\langle\psi|\hat{p}|\psi\rangle \geq 0$ for $\psi \in \mathcal{R}$ and so the inequality vanishes. Thus the spatial extent of backflow is restricted and state-independent.

It is quite remarkable that there exist both spatial and temporal limitations on backflow. Is there a relationship between them? Does one impose a stronger constraint on backflow than the other? These are interesting questions that could form the basis for future work. The inequality Eq.(3.11) demonstrates that backflow is restricted in space, but is there any way to give a quantitative measure of the fraction of the x-axis over which the effect takes place? It is this question that we will address now.

3.3 A Measure of the Spatial Extent of Backflow

Quantum weak measurements challenge the notion that non-commuting observables cannot be simultaneously measured. If the coupling with the measuring device is sufficiently weak, properties of a quantum state can be determined without disturbing the system. The result of such a measurement defines a new kind of value for a quantum variable known as a weak value [23]. For a bounded operator $\hat{A}$, the weak value of a measurement depends not only on the preselected state $|\psi\rangle$, but also the postselected

state $|\phi\rangle$. That is to say,

$$A_{weak} = \frac{\langle\phi|\hat{A}|\psi\rangle}{\langle\phi|\psi\rangle} \tag{3.17}$$

A weak measurement of the momentum operator $\hat{p}$ in the preselected state $|\psi\rangle$, with the state $|\phi\rangle = |x\rangle$ postselected, can be shown to yield the local wavenumber $k(x)$ [5],

$$A_{weak} = \mathrm{Re}\frac{\langle x|\hat{p}|\psi\rangle}{\langle x|\psi\rangle} = k(x) \tag{3.18}$$

where

$$k(x) = \mathrm{Im}\frac{\partial\psi(x)/\partial x}{\psi(x)} \tag{3.19}$$

Backflow occurs in certain regions of the x-axis where $k(x) < 0$. The fraction of the x-axis for which $k(x) < 0$ is characterised by the backflow probability P_{back}, defined as

$$\begin{aligned} P_{back} &= \lim_{L\to\infty}\frac{1}{2L}\int_{-L}^{L}\mathrm{d}x\,\Theta(-k(x)) \\ &= \int_{-\infty}^{0}\mathrm{d}k\,P_k(k) \end{aligned} \tag{3.20}$$

where Θ is the Heaviside step function, P_k is the probability density of the local wavenumber, that is

$$P_k(k) = \lim_{L\to\infty}\frac{1}{2L}\int_{-L}^{L}\mathrm{d}x\,\delta(k - k(x)) \tag{3.21}$$

and it is useful to define the wavenumber $k = p/\hbar$. P_{back} is a measure of the backflowing regions on the x-axis; an indication of the spatial extent of the negative current. This is very similar to the smeared current Eq.(3.3), which represents the current measured over a spatially extended region of the x-axis.

Weak measurements of the operator $\hat{A}$ with eigenvalues A_n symmetrically distributed in the range $-A_{max} \leq A_n \leq +A_n$ yields the probability distribution of weak values, $P(A_{weak})$. For randomly chosen preselected and postselected states this has the form [24],

$$P(A_{weak}) = \frac{\langle A_n^2\rangle}{2\left(A_{weak}^2 + \langle A_n^2\rangle\right)^{3/2}} \tag{3.22}$$

where now $\langle\ldots\rangle$ denotes an ensemble average and not a quantum expectation value as before. By restricting the distribution to only positive semidefinite wavenumbers, we can write,

$$A_{weak} = -A_{max} + k, \qquad A_n = -A_{max} + k_n \tag{3.23}$$

and Eq.(3.22) may be expressed as

$$P_k(k) = \frac{\langle k_n^2\rangle - \langle k_n\rangle^2}{2\left(k^2 - 2k\langle k_n\rangle + \langle k_n^2\rangle\right)^{3/2}} \tag{3.24}$$

Here,

$$\langle k_n \rangle = \frac{\sum_{n=0}^{N} |C_n|^2 k_n}{\sum_{n=0}^{N} |C_n|^2}, \qquad \langle k_n^2 \rangle = \frac{\sum_{n=0}^{N} |C_n|^2 k_n^2}{\sum_{n=0}^{N} |C_n|^2} \tag{3.25}$$

and C_n is a complex coefficient of the state $|\psi\rangle$. The backflow probability, Eq.(3.20), can now be defined as

$$P_{back} = \frac{1 - r_{back}}{2} \tag{3.26}$$

where

$$r_{back} \equiv \frac{\langle k_n \rangle}{\sqrt{\langle k_n^2 \rangle}} \tag{3.27}$$

This is an important result that shows a relationship between the distribution of component momenta, $p_n = \hbar k_n$, in the wavepacket and the fraction of the x-axis over which backflow occurs. If the spread is larger, then P_{back} increases and approaches its maximum value of a $1/2$ when $\langle k_n^2 \rangle \gg \langle k_n \rangle^2$. We now possess a quantitative measure of the spatial extent of backflow that can be applied to any state provided the distribution of its component momenta is known. For the experimental realisation of backflow, P_{back} could be extremely useful in helping plan a measurement of the effect.

To illustrate the material presented in this section, a plot of the local wavenumber $k(x)$ against x is shown in Fig.(3.1) for a wavefunction of the form,

$$\psi(x) = \sum_{n=1}^{20} \frac{1}{\sqrt{n}} \exp[i(nx + \phi_n)] \tag{3.28}$$

where ϕ_n is a phase factor randomly chosen from the interval $[0, 2\pi]$.

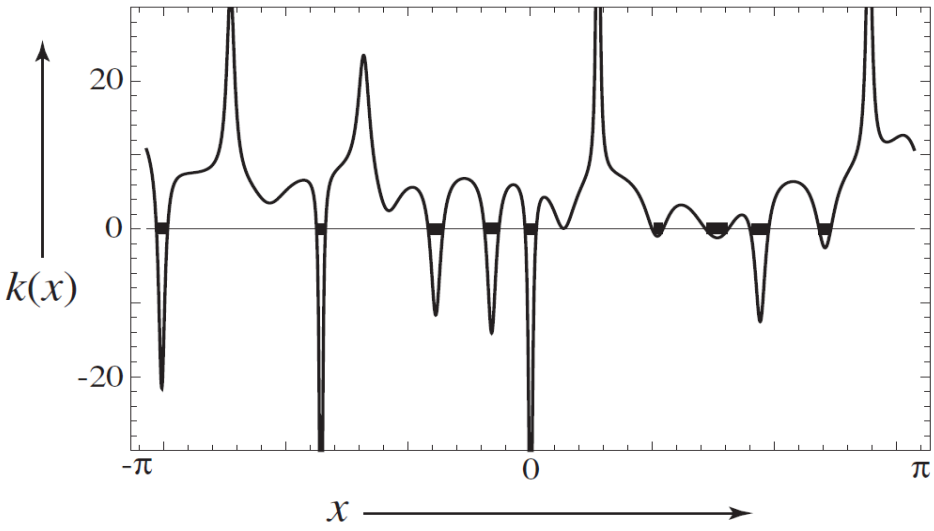

Figure 3.1: Plot of the local wavenumber $k(x)$, for the 20-wave superposition Eq.(3.28). The regions of backflow are indicated by black bars [5].

Fig.(3.1) provides a clear way of visualising the regions of backflow on the x-axis. For this 20-wave superposition, which is periodic in x with period 2π, there are nine backflow regions per period. Using Eq.(3.26), the backflow probability $P_{back} = 0.136$.

3.4 Strong Backflow and Superoscillations

Backflow is related to the phenomenon of superoscillations, a seemingly paradoxical effect in which waves can locally oscillate much faster than any components in their Fourier spectrum [22]. The fast oscillations in an associated function are dependent on the preselected and postselected states of a weak measurement [25]. It is the weak values which lie outside the allowed eigenvalue spectrum that give rise to this counterintuitive effect. It was Berry [5] who brought attention to the relationship between backflow and superoscillations but it has not been explored elsewhere in the literature. Certainly there are parallels between the two. Superoscillations can be arbitrarily fast and can persist for unexpectedly long times occupying large regions of the x-axis [26]. As we saw in Sec.(2.3) the current can be arbitrarily negative if only for a sufficiently short time, indicating in a way, that backflow can be 'abitrarily fast'. In contrast, it is also true that a period of backflow can be arbitrarily long.

In many-wave superpositions when the Fourier components are strongly correlated, the region of backflow is much larger than if the components were randomly distributed. The backflowing fraction of the x-axis characterised by P_{back} approaches its maximum value of 1/2 and the state displays "strong backflow". To demonstrate this, consider the wave function

$$\psi_{strong}(x) = (1 - a\exp(ix))^N, \qquad N \gg 1, \qquad a < 1 \tag{3.29}$$

which is a variant of the superoscillatory function [26],

$$f(x) = (\cos(x) + ib\sin(x))^N, \qquad N \gg 1, \qquad b > 1 \tag{3.30}$$

For $f(x)$ when $b > 1$, the variation near $x = 0$ is faster and so,

$$f(x) \approx \exp\left(N\log(1 + ibx)\right) \approx \exp(ibNx) \tag{3.31}$$

where b describes the degree of superoscillation. Around this region, the amplitude of superoscillations is approximately constant and $f(x)$ exhibits "fast superoscillations". A similar effect occurs in ψ_{strong} near $x = 0$ for $a < 1$, the largest backflow occuring when the local wavenumber is,

$$k(0) = -\frac{Na}{1-a} \tag{3.32}$$

The corresponding backflowing fraction of the x-axis is,

$$P_{back} = \frac{\cos^{-1}(a)}{\pi} \tag{3.33}$$

which is far higher than the value predicted using Eq.(3.26) for a random distribution,

$$P_{back} \approx \frac{1}{8Na} \tag{3.34}$$

However, evolution of the state according to the Schrödinger equation results in the destruction of the phases responsible for strong backflow. The region of backflow shrinks and becomes comparable in size to that of a random superposition. This is shown in Fig.(3.2). The strong backflow region gradually decreases but undergoes a quantum revival [27] at $t = 2\pi$ due to the inital state $\psi_{strong}(x)$ being periodic. The destruction of strong backflow is consistent as N increases, best shown by considering Fig.(3.3).

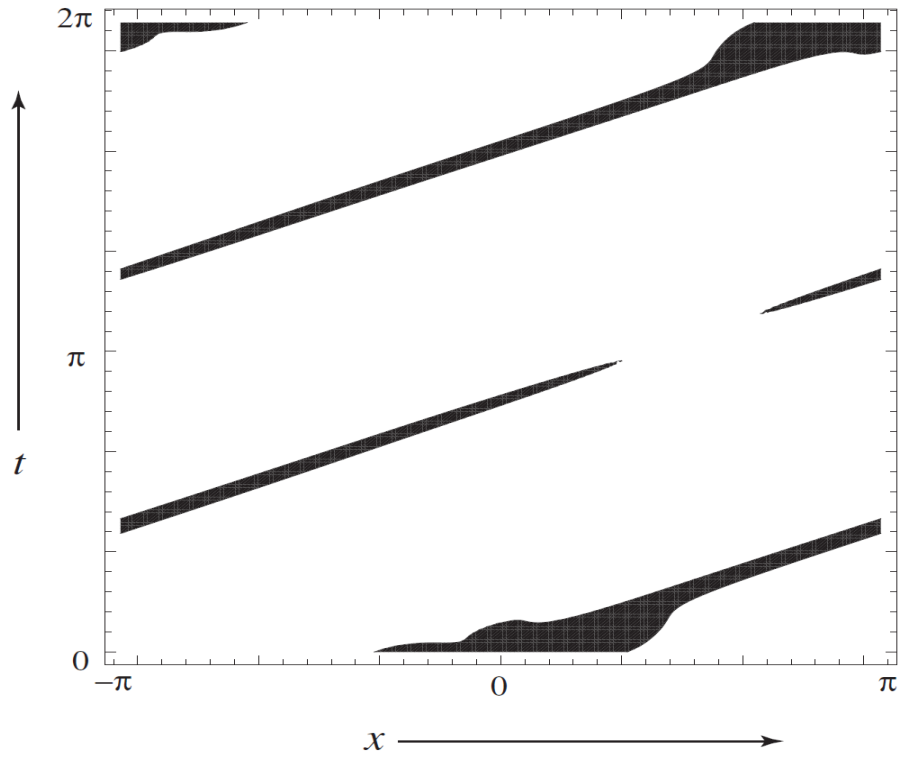

Figure 3.2: Evolution of the strong backflowing state ψ_{strong} with $a = 0.5$ and $N = 6$ [5].

A similar process occurs with superoscillations. If we treat $f(x)$ as the initial state of a wave function in free space undergoing evolution according to the Schrödinger equation, then eventually the superoscillations disappear [26]. This is due to the component momenta becoming exponentially different in magnitude during the time evolution of the state.

Backflow and superoscillations are examples of counterintuitive quantum phenomena which on closer inspection have striking similarities. It is known that fast superoscillations occur in regions where the amplitude of the function $f(x)$ is small [28], and so one might speculate that strong backflow is only evident in small negative flux states where the component momenta are strongly correlated.

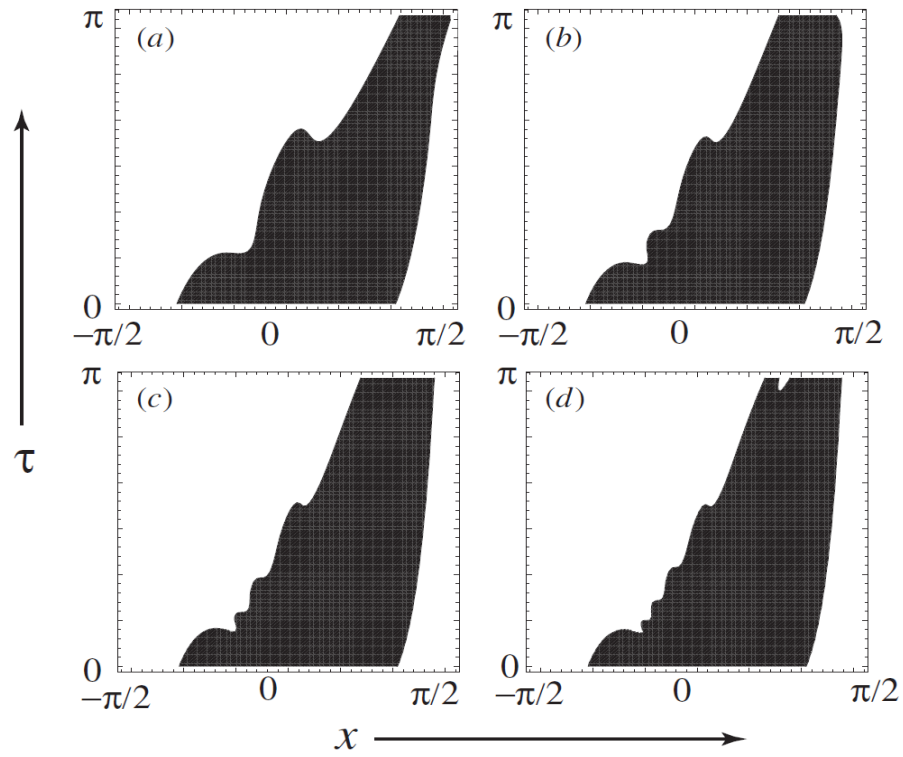

Figure 3.3: Destruction of strong backflow in the initial stages of evolution for the state ψ_{strong} with $a = 0.5$ and (a) $N = 6$, (b) $N = 10$, (c) $N = 14$, (d) $N = 18$. Here $\tau = Nt$ [5].

4 States Which Display Backflow

4.1 Introduction

Not every quantum state exhibits backflow, and so an interesting set of questions concerns the type of state which does. It is often useful to look at the Wigner function W, of a state since negative values of W give a clear indication of non-classical behaviour. However as we saw in Sec.(2.1) this is not a sufficient condition for the negativity of the flux, therefore a more detailed analysis is required.

Bracken and Melloy [3] presented the first comprehensive computation of a normalisable state which displays backflow. Although physically significant, the wave function chosen was not reflective of a realistic state and produced only a small fraction of the maximum possible backflow. Plane waves have frequently been used in the literature to illustrate the backflow effect [1, 3, 5]. The most interesting application was by Berry [5] who found that in many-wave superpositions in which the component momenta are strongly correlated, the state will exhibit strong backflow.

In their work on the arrival time problem, Muga et al used the example of a Gaussian in momentum space with no negative momentum components [10]. The corresponding wave function in configuration space is described by,

$$\psi(x,t) = \frac{1}{(2\pi\hbar)^{1/2}} \int_0^\infty \mathrm{d}p \, \exp\left(\frac{i}{\hbar}\left(px - \frac{p^2 t}{2m}\right)\right) \langle p|\phi_{in}(0)\rangle \tag{4.1}$$

where $\langle p|\phi_{in}(0)\rangle$ is a freely evolving asymptote associated with scattering theory. This is not a simple function and due to conditions placed on the magnitude of the momenta, the amount of backflow displayed is far from the theoretical maximum. The example served only to demonstrate the effect and that it is possible for a perfect absorber to emit probability. Since their analysis focused more on the operational arrival time distribution and the relationship between backflow and perfect absorption, we will not study this state further but refer the reader to Ref.[10].

Important contributions have been made by Yearsley et al [1]. They found that a more physically realistic state consisting of a superposition of two Gaussian wavepackets will display around 16% of the maximum possible backflow. Although small, their work begins to address the long standing problem of what type of state could be used to observe backflow experimentally. Also investigated was an analytic expression for the backflow maximising state. It is encouraging that attempts have been made to find an analytic solution to the eigenvalue equation Eq.(2.19), as this problem underpins the whole subject of backflow.

In this chapter we focus on states that have been significant in the advancement of the subject. A superposition of two plane waves will demonstrate that negative values of the current can be understood as an interference effect. The more familiar example of a superposition of two Gaussian wavepackets is examined as this has the potential to be experimentally realised. We will study the normalisable state first presented by

Bracken and Melloy. Finally, an analytic expression for the backflow maximising state put forward by Yearsley et al will be reviewed. Note that a Schrödinger cat state will also produce backflow but since its preparation is closely related to the experimental realisation of the effect, we save the analysis for Chapter 6. It should be emphasised that regardless of the type of state which displays backflow, after a sufficiently long period of time a large proportion of the wave packet will be located in $x > 0$ [3].

4.2 Superposition of Plane Waves

It is informative to consider a superposition of two plane waves with positive momenta described by the wave function,

$$\psi_{plane}(x,t) = \sum_{n=1,2} C_n \exp[ip_n(x - p_n t)], \quad C_n \in \mathbb{R} \tag{4.2}$$

where for convenience we choose $h = m = 1$. Since ψ_{plane} cannot be normalised, these results have no direct physical interpretation but serve to illustrate the backflow effect.

The probability current, Eq.(2.2), at $x = 0$ for ψ_{plane} is

$$J(0,t) = C_1^2 p_1 + C_2^2 p_2 + C_1 C_2 (p_1 + p_2) \cos[(E_1 - E_2)t] \tag{4.3}$$

This oscillates between a maximum value of $(C_1 p_1 + C_2 p_2)(C_1 + C_2)$ and a minimum value of $(C_1 p_1 - C_2 p_2)(C_1 - C_2)$. If however, $C_1 > C_2$ and $C_1 p_1 < C_2 p_2$, the minimum value is negative and the state displays backflow. This example demonstrates that negative values of J can be understood as an interference effect. A plot of the current at the origin is shown in Fig.(4.1) for the following parameters,

$$p_1 = 0.3, \qquad p_2 = 1.4, \qquad C_1 = 1.8, \qquad C_2 = 1 \tag{4.4}$$

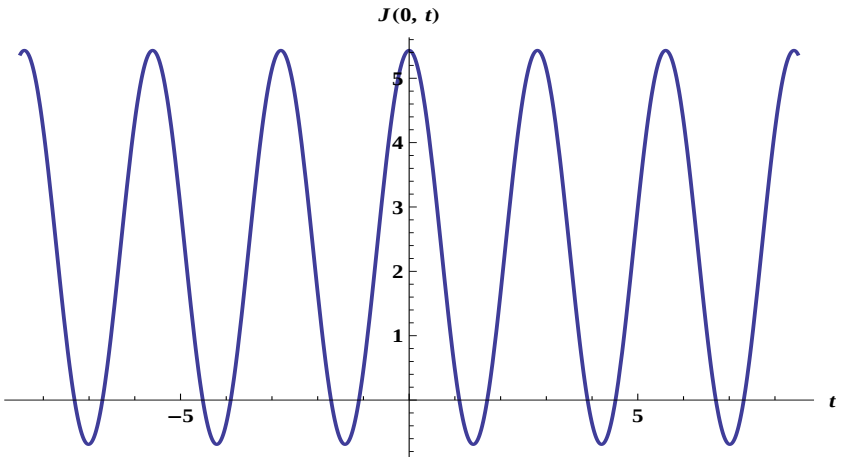

Figure 4.1: Plot of $J(0,t)$ for a superposition of two plane waves with the parameters given in Eq.(4.4).

We will now show the relationship that emerges between the local wavenumber $k(x)$ of ψ_{plane} and the region of backflow on the x-axis. If we choose a specific moment in time during a period of backflow and change the parameters to,

$$p_1 = 0, \qquad p_2 = 1, \qquad C_1 = 1, \qquad C_2 = a \tag{4.5}$$

then ψ_{plane} is now of the form,

$$\psi_{plane}(x) = 1 - a\exp(ix) \tag{4.6}$$

and has local wavenumber,

$$k(x) = a\frac{(a - \cos(x))}{1 + a^2 - 2a\cos(x)} \tag{4.7}$$

This periodic function displays backflow for values of $a < 1$, within the interval $|x| < \cos^{-1}(a)$. Berry [5] studied how the width of the region of backflow changes for varying values of a and we show his results in Fig.(4.2).

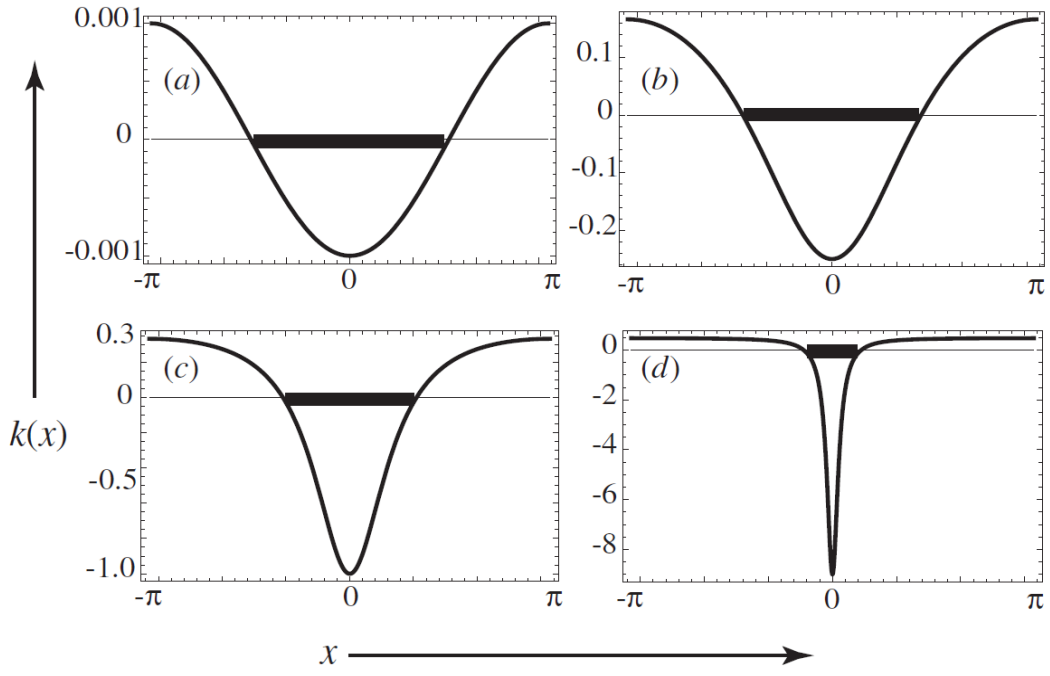

Figure 4.2: Plot of the local wavenumber $k(x)$, Eq.(4.7), for the two-wave superposition Eq.(4.6). The regions of backflow are indicated by black bars, for (a) $a = 0.001$, (b) $a = 0.2$, (c) $a = 0.5$, (d) $a = 0.9$. The width of the region of backflow increases as a decreases and the degree of backflow decreases, i.e. as $k(x)$ gets less negative [5].

It is quite striking to see the width of the region of backflow increase as a decreases. In the limit $a \to 0$, the region grows and covers half of the x-axis even though the negative flux is getting smaller and the amount of backflow is actually decreasing. The

backflow probability P_{back} is the probability a given x lies in a region of backflow, and for ψ_{plane} this is,

$$P_{back} = \frac{\cos^{-1}(a)}{\pi} \tag{4.8}$$

4.3 Superposition of Gaussian Wavepackets

The replacement of plane waves with Gaussians tightly peaked in momentum is representative of a more physically realistic state that has the potential to be experimentally realised [1]. We consider a sum of two initial Gaussian wavepackets with equal spatial width σ, evolved for a time t. The corresponding normalised wave function is

$$\psi(x,t) = \sum_{n=1,2} C_n \frac{1}{\sqrt{4\sigma^2 + 2it}} \exp\left(ip_n(x - p_n t) - \frac{(x - p_n t)^2}{4\sigma^2 + 2it} \right), \quad C_n \in \mathbb{R} \tag{4.9}$$

where again we set $h = m = 1$. It is important that the state is normalised to ensure the flux is properly normalised. Note that if $\sigma \to \infty$ then $\psi \to \psi_{plane}$. By making σ large enough, the current at $x = 0$ is the product of Eq.(4.3) and a slowly varying function. One would therefore expect ψ to exhibit backflow just like ψ_{plane}. Yearsley et al [1] found the parameters

$$p_1 = 0.3, \quad p_2 = 1.4, \quad C_1 = 1.8, \quad C_2 = 1, \quad \sigma = 10 \tag{4.10}$$

produced the greatest amount of backflow for a superposition of two Gaussian wavepackets as described by Eq.(4.9). The current at the origin is clearly negative at several times as can be seen in Fig.(4.3).

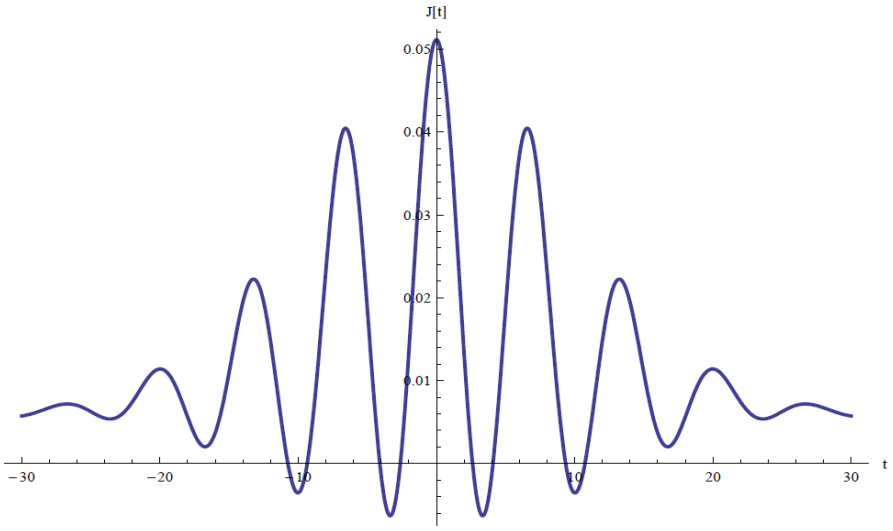

Figure 4.3: Plot of the current at $x = 0$ for a superposition of two Gaussian wavepackets [1] with the parameters given in Eq.(4.10).

If we plot the probability of remaining in $x < 0$ as a function of time, it is apparent that backflow can occur in several disjoint time intervals, as shown in Fig.(4.4).

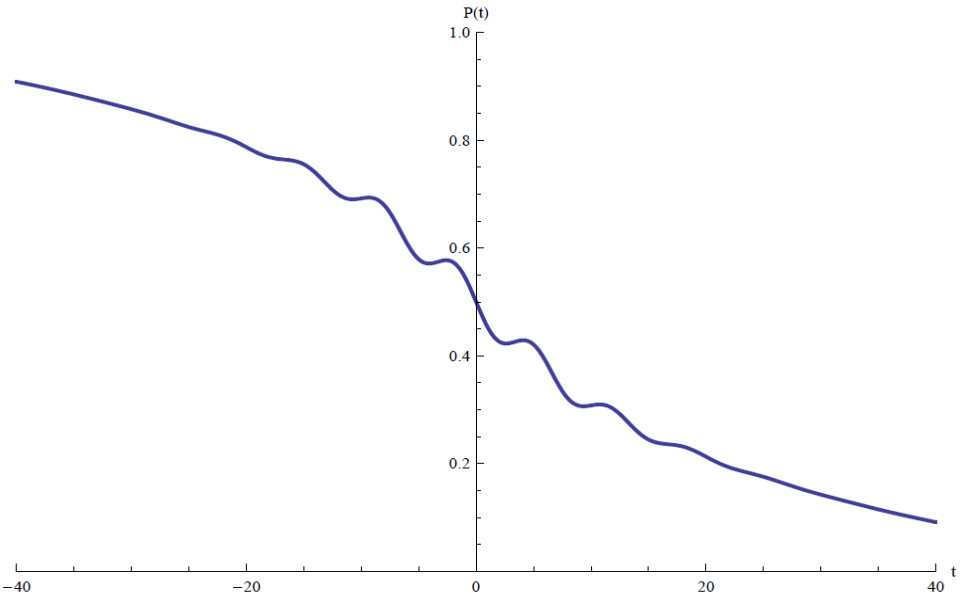

Figure 4.4: Plot of the probability for remaining in $x < 0$ as a function of time for a superposition of two Gaussian wavepackets [1].

The question is now; how much probability backflow does this state display in comparison to the theoretical maximum value of c_{bm}? To answer this the flux, Eq.(2.6), must be calculated for a time interval $[t_1, t_2]$, during which the current is negative and the largest amount of backflow occurs. Calculations show that,

$$F \approx -0.0061 \tag{4.11}$$

which is around 16% of the theoretically allowed maximum. The fraction of the x-axis over which backflow occurs for this state is,

$$P_{back} = 0.1162 \tag{4.12}$$

A strong indication of the non-classicality of this state is that the Wigner function of a superposition of Gaussians may be negative in certain regions. However, Gaussian wavepackets have support on both positive and negative momentum so the presence of negative current could be a result of some initial negative momentum. It is therefore necessary to check this is not the case by making an order of magnitude estimate.

The state consists of two Gaussian wavepackets centred about different momenta. If we take the wavepacket centred around $p = 0.3$, then the probability that a measurement of the momentum of this state would produce a negative answer is approximately,

$$\Pr(p < 0) \sim \int_{-\infty}^{0} \mathrm{d}p \, \exp(-200(p - 0.3)^2) \sim 10^{-10} \tag{4.13}$$

which is negligible. The backflow effect is therefore responsible for the negative flow of probability.

4.4 A Normalisable State

We focus our attention to the state first presented by Bracken and Melloy [3] which is described by the wave function,

$$\psi_{bm}(x,t) = \frac{1}{(2\pi\hbar)^{1/2}} \int_0^\infty \mathrm{d}p \, \exp\left(\frac{i}{\hbar}\left(px - \frac{p^2 t}{2m}\right)\right) \phi(p) \tag{4.14}$$

where $\phi(p) = 0$ for $p < 0$, or else

$$\phi(p) = \frac{18p}{(35K)^{1/2}} \left(e^{-p/K} - \frac{1}{6}e^{-p/2K}\right), \qquad p > 0 \tag{4.15}$$

Here, K is a positive constant with dimensions of momentum. Both $\psi_{bm}(x,t)$ and $\phi(p)$ are normalised states, therefore we may regard ψ_{bm} as having a direct physical interpretation. It is unlikely however that a state of the form Eq.(4.14) would ever appear in nature, so although this example demonstrates backflow it should not be thought of as a realistic state in the strict sense.

The current Eq.(2.2) at the origin, for ψ_{bm} has the form,

$$J(0,t) = \frac{1}{4\pi m\hbar} \int_0^\infty \mathrm{d}p \int_0^\infty \mathrm{d}q \, (p+q) \exp\left(\frac{i}{2m\hbar}\left(p^2 - q^2\right) t\right) \phi^*(p)\phi(q) \tag{4.16}$$

which when calculated at $t = 0$ is

$$J(0,0) = -\frac{36K^2}{35\pi m\hbar} < 0 \tag{4.17}$$

The current is negative during the time interval $[0, t_1]$ where $t_1 \approx 0.021 m\hbar^2/K^2$. The corresponding flux Eq.(2.6), for this period of backflow is

$$F \approx -0.0043 \tag{4.18}$$

which is around 11% of the theoretical maximum. This is a very small amount but it is momentous. What Bracken and Melloy have demonstrated by using a normalisable wave function is that backflow is a physically relevant quantum effect which can occur in non-relativistic free particles. The implications of this were already evident in the arrival time problem, but Allcock [2] failed to give the effect the appropriate weight it deserved. Although Allcock will be regarded as the one who discovered the backflow effect, it is Bracken and Melloy who revealed its true significance.

4.5 Guessing the Analytic Form of the Backflow Maximising State

It is of great interest to find the analytic expression for the backflow maximising state. By a process of logical guesswork, Yearsley et al [1] proposed two analytic candidate states, one of which showed greater promise. In this section we look at this state and see that although it appears to match the numerical results of the backflow maximising state by Penz et al [8], it does not exhibit the maximum possible backflow.

We consider the momentum space wave function $\phi_g(u)$ given by,

$$\phi_g(u) = N\left[ae^{-bu}\left(\frac{1}{2} - C(u)\right)\right], \quad a, b \in \mathbb{R} \tag{4.19}$$

where N is a normalisation factor which can be calculated by solving the integral,

$$N^{-2} = \int_0^\infty \mathrm{d}u \left(a^2 e^{-2bu} + \left(\frac{1}{2} - C(u)\right)^2 + 2ae^{-bu}\left(\frac{1}{2} - C(u)\right)\right) \tag{4.20}$$

and $C(u)$ is the Fresnel integral, defined by

$$C(u) = \mathrm{FresnelC}\left(\sqrt{\frac{2}{\pi}}u\right) = \sqrt{\frac{2}{\pi}}\int_0^u \mathrm{d}x\, \cos(x^2) \tag{4.21}$$

A plot of $\phi_g(u)$ in momentum space for the optimum values of a and b to maximise backflow is shown in Fig.(4.5).

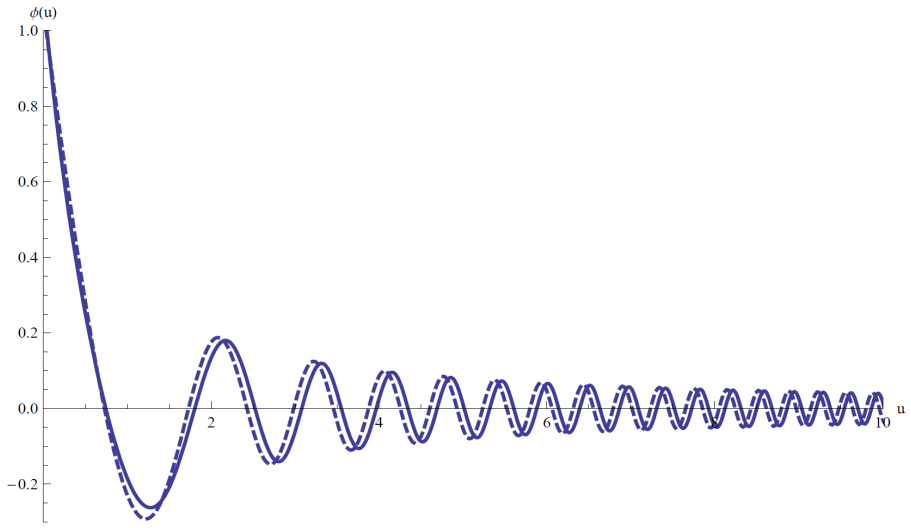

Figure 4.5: Plot of $\phi_g(u)$ for $a = 0.6$ and $b = 2.8$ (solid line), compared with the numerical result (dashed line) [1].

This state has the asymptotic form,

$$\phi_g(u) \sim N\frac{\sin(u^2)}{u} \tag{4.22}$$

Since $\phi_g(u)$ is only an approximate eigenstate of the flux operator, the time interval over which the current is negative may not exactly match $[-1, 1]$. It is therefore necessary to adjust the the time interval $[t_1, t_2]$ to correspond with the period of negative flux. The current, defined in terms of the dimensionless parameters u and v, is

$$J(0,t) = \frac{1}{2\pi}\int_0^\infty \mathrm{d}u\,\mathrm{d}v\,(u+v)\exp\left(it(u^2+v^2)\right)\phi(u)\phi(v) \tag{4.23}$$

which may can also be expressed as,

$$\begin{aligned} J(0,t) &= \mathrm{Re}\left(\frac{1}{\pi}\int_0^\infty \mathrm{d}u\,\exp(itu^2)\phi(u)\int_0^\infty \mathrm{d}v\,v\exp(-itv^2)\phi(v)\right) \\ &= \frac{1}{\pi}\mathrm{Re}\left(U(t)V(t)\right) \end{aligned} \tag{4.24}$$

The process to calculate the current Eq.(4.24), is reduced to solving the two integrals $U(t)$ and $V(t)$ separately. (See Ref.[1] for a detailed solution to the problem). We plot the current as a function of time in Fig.(4.6).

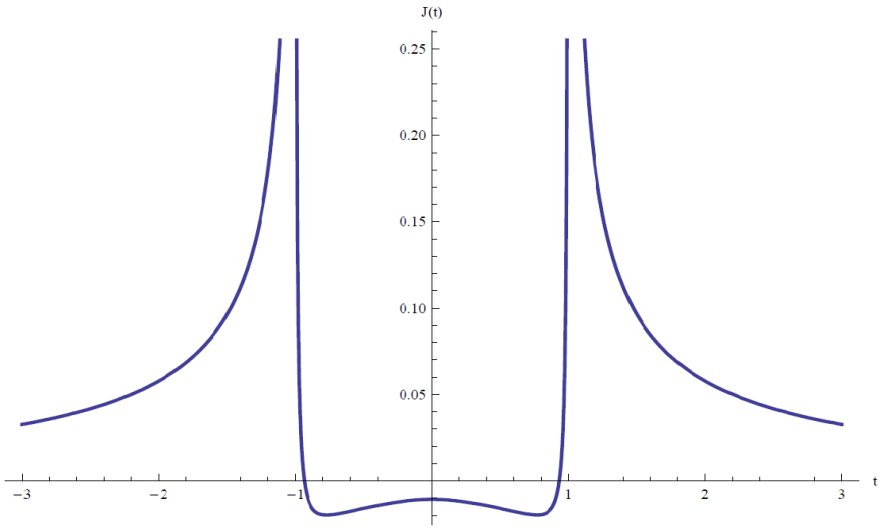

Figure 4.6: Plot of $J(0,t)$ for the state $\phi_g(u)$ with $a = 0.6$ and $b = 2.8$ [1].

The plot of $J(0,t)$ is in good agreement with the numerical result Fig.(2.3) but does not possess the distinct singularity structure at $t = \pm 1$. There is however a significant period of backflow clearly indicted by the negativity of the current between the interval $[-1, 1]$. The most negative value of the flux, Eq.(2.14), is

$$F = -0.02757 \tag{4.25}$$

which is around 70% of the theoretical maximum. This state displays a much greater amount of backflow than any other analytic state previously discovered, however it is still much less than the backflow maximising state.

A plot of the probability for remaining in $x < 0$ as a function of time, for the guess state $\phi_g(u)$, can be seen in Fig.(4.7). This is a very striking illustration of backflow which unequivocally demonstrates the effect. There is a clear increase of probability within the time interval $[-1, 1]$ when the current is negative.

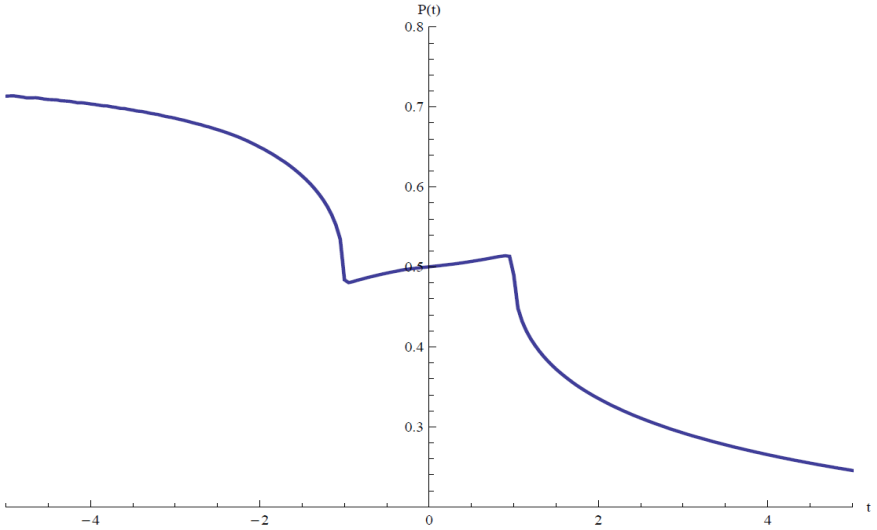

Figure 4.7: Plot of the probability $P(t)$ for remaining in $x < 0$ as a function of time for the guess state $\phi_g(u)$ [1].

It would be of great interest to find and plot the configuration space wave function of $\phi_g(u)$ and compare it with that of the backflow maximising state computed by Penz et al [8] as shown in Fig.(2.2). A direct comparison may provide clues as to how the form of the momentum space wave function must be modified in order to display a greater percentage of backflow. The singularity structure of the current at $t = \pm 1$ is another characteristic that has failed to be matched. Any future work must focus on an analytic solution that possesses this structure.

5 A New Quantum Number

5.1 Introduction

The appearance of the dimensionless quantity c_{bm} in the quantum mechanical description of a free particle is itself remarkable. The fact this number describes a limit on backflow is not surprising, for if there was no restriction then increasing amounts of probability could flow "backwards" and the situation would certainly be more alarming. What is striking about c_{bm} is its independence from the parameters $\hbar, m$ and T. One does not expect this value to be independent of the duration of the time interval over which backflow occurs, nor of the mass of the particle. The independence from $\hbar$ also raises concerns about how this strictly quantum effect ceases to exist in classical systems. In the naive classical limit $\hbar \to 0$, backflow does not go away as one would hope.

Backflow is an interference effect between parts of the state that have crossed the origin, and parts which have yet to cross. As noted earlier in open system models, these interference effects are suppressed by the presence of an environment and backflow ceases to occur [13]. The process of decoherence is a central idea in the understanding of emergent classicality and provides good insight into why backflow disappears in the standard approach to the classical limit. There are however certain situations where the eigenvalues of the flux operator Eq.(2.12), in particular the most negative eigenvalue $-c_{bm}$, become dependent on certain physical parameters, most notably $\hbar$.

In this chapter we consider a more realistic measurement model [1], where the use of quasiprojectors instead of exact projection operators restores the naive classical limit, and the backflow effect diminishes when $\hbar \to 0$. So far we have only focused on the non-relativistic behaviour of a particle, but this must correspond to a limiting case of its relativistic description. For particles governed by the Dirac equation [4], it will be shown that the amount of backflow depends on the dimensionless combination $mc^2T/\hbar$, where c is the speed of light. It has been speculated that particles might literally for some time intervals masquerade as antiparticles [5].

Finally, we study the case of a particle subject to a constant force $F > 0$ in the positive x-direction and ask how much probability backflow can occur in opposition to this force over a given time interval [6]. Here, the effect of backflow gets smaller when the size of the force is increased.

5.2 Quasiprojector Measurement Model

A measurement to determine if the particle is in $x > 0$ at time t_1, and then at a subsequent time t_2, could lead to the observation of backflow if the flux,

$$F(t_1, t_2) = \langle \Pi(t_2) \rangle - \langle \Pi(t_1) \rangle \tag{5.1}$$

expressed in terms of the exact projection operator $\Pi = \theta(\hat{x})$, is negative. However the use of exact projection operators does not incorporate the inherent imprecision of real measurements. Instead, one may choose to define the flux in terms of a quasiprojector Q, which is perhaps more representative of a realistic measurement model. Quasiprojectors are self-adjoint operators but since they do not satisy the property, $Q^2 = Q$, they are not projection operators in the strict sense. For our purposes, we define a quasiprojector

$$Q = \int_0^\infty \mathrm{d}y \, \delta_\sigma(\hat{x} - y) \tag{5.2}$$

where $\delta_\sigma(\hat{x} - y)$ is a smoothed out δ-function,

$$\delta_\sigma(\hat{x} - y) = \frac{1}{(2\pi\sigma^2)^{1/2}} \exp\left(-\frac{(\hat{x} - y)^2}{2\sigma^2}\right) \tag{5.3}$$

and σ is a physical parameter characterizing the imprecision of real measurements. Note that if $\sigma \to 0$, then $Q \to \theta(\hat{x})$ and Eq.(5.3) goes to the usual δ-function. The introduction of Q means the flux, as expressed in Eq.(2.20), is now

$$F(-T/2, T/2) = \frac{1}{\pi} \int_0^\infty \mathrm{d}u \int_0^\infty \mathrm{d}v \, \phi^*(u) \frac{\sin(u^2 - v^2)}{(u - v)} e^{-a^2(u-v)^2} \phi(v) \tag{5.4}$$

and the eigenvalue equation Eq.(2.19), obtains the same exponential factor,

$$\frac{1}{\pi} \int_0^\infty \mathrm{d}v \, \frac{\sin(u^2 - v^2)}{(u - v)} e^{-a^2(u-v)^2} \phi(v) = \lambda \phi(u) \tag{5.5}$$

where a is a dimensionless quantity given by $a^2 = 2m\sigma^2/\hbar T$. The eigenvalues λ will now depend on a, and thus have a dependence on $\hbar$.

The limit on the total amount of backflow, $\Delta_{max}(a)$, is equal to the most negative eigenvalue of Eq.(5.5). Using numerical methods, Yearsley et al [1] solved Eq.(5.5) to look at how $\Delta_{max}(a)$ varies for increasing a. The results are displayed in Fig.(5.1). In the naive classical limit $\hbar \to 0$, $a \to \infty$ and $\Delta_{max}(a) \to 0$. This is significant as it suggests that backflow diminishes in the more realistic measurement model of quasiprojectors when $\hbar \to 0$. Note that $\Delta_{max}(a)$ is still negative for finite a, so although the amount of backflow is less, the effect is still noticeable and could be measured.

Approximate eigenstates of Eq.(2.19) will have eigenvalues 1 or 0 provided the wave packets they consist of clearly cross or do not cross $x = 0$ during the interval $[-T/2, T/2]$. For the modified eigenvalue equation Eq.(5.5), there is an additional requirement. An incoming wave packet will not distinguish a projector from a quasiprojector as long as it crosses $x = 0$ far enough away from the end-points of the interval $[-T/2, T/2]$. Yearsley et al [1] found that the positive eigenvalues in the range $[0, 1]$ do not significantly change as a increases. If they had converged to zero, the results concerning $\Delta_{max}(a)$ would be meaningless. Since this is not the case, we can regard the use of quasiprojectors as being a relevant description of the measurement process, where one would expect backflow to vanish in the appropriate classical limit.

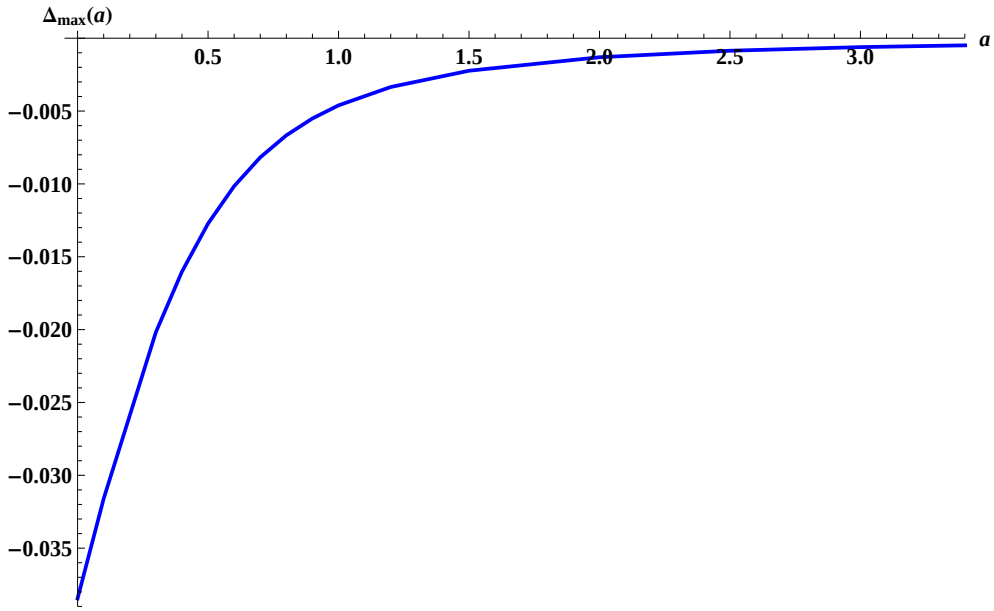

Figure 5.1: Plot of the most negative eigenvalue of Eq.(5.5), $\Delta_{max}(a)$ for increasing a.

5.3 Backflow for a Free Dirac Electron

The description of backflow presented so far has concentrated on the non-relativistic behaviour of a particle. Since this must correspond to a limiting case of its relativistic description [4], we now ask the question: How does probability backflow manifest itself in the relativistic case?

It will suffice to consider a free Dirac electron moving in one dimension along the x-axis. The corresponding wave function has two complex-valued components,

$$\Psi(x,t) = \begin{pmatrix} \psi_1(x,t) \\ \psi_2(x,t) \end{pmatrix} \tag{5.6}$$

and we have a Dirac equation in $(1+1)$ dimensions,

$$i\hbar \frac{\partial \Psi(x,t)}{\partial t} = H\Psi(x,t) \tag{5.7}$$

where the Hamiltonian,

$$H = c\sigma_1 p + \sigma_3 mc^2 \tag{5.8}$$

is expressed in terms of the Pauli matrices σ_i, the rest mass of the particle m, and the speed of light c. The probability density ρ, and probability current J, then have the form,

$$\begin{aligned} \rho(x,t) &= \Psi^\dagger(x,t)\Psi(x,t) \\ &= |\psi_1(x,t)|^2 + |\psi_2(x,t)|^2 \end{aligned} \tag{5.9}$$

and

$$J(x,t) = c\Psi^{\dagger}(x,t)\sigma_1\Psi(x,t)$$
$$= c\left[\psi_1^*(x,t)\psi_2(x,t) + \psi_2^*(x,t)\psi_1(x,t)\right] \tag{5.10}$$

Note that $|J(x,t)| \leq c\rho(x,t)$, which means that the probability velocity $v(x,t)$, defined by

$$v(x,t) = \frac{J(x,t)}{\rho(x,t)} \tag{5.11}$$

satisfies $|v(x,t)| \leq c$. This ensures that there is no superluminal transport of probability associated with the free Dirac equation.

The process to determine the limit on the total amount of backflow is similar to the non-relativistic case. Here, a general positive energy and positive momentum solution to the Dirac equation is used to determine the probability current, Eq.(5.10), at $x = 0$. For the time interval $[0, T]$, the limit on the total amount of backflow, $\Delta_{max}(\epsilon)$, is then equal to the most negative eigenvalue of the equation,

$$\frac{1}{\pi}\int_0^{\infty} \mathrm{d}v\, \frac{\sin[2(\mathcal{E}(u)-\mathcal{E}(v))/\epsilon^2][u(\mathcal{E}(v)+1)+v(\mathcal{E}(u)+1)]}{[2(\mathcal{E}(u)-\mathcal{E}(v))/\epsilon^2]\sqrt{\mathcal{E}(u)(\mathcal{E}(u)+1)\mathcal{E}(v)(\mathcal{E}(v)+1)}}\Phi(v) = \lambda\Phi(u) \tag{5.12}$$

where

$$\mathcal{E}(u) = \frac{\sqrt{p^2+m^2c^2}}{mc}, \qquad p = mc\epsilon u \tag{5.13}$$

and

$$\epsilon = \sqrt{\frac{4\hbar}{mc^2T}} \tag{5.14}$$

By letting $c \to \infty$, so that $\epsilon \to 0$ and $\mathcal{E}(u) \to 1 + \epsilon^2u^2/2$, we recover the non-relativistic eigenvalue equation for a free particle, Eq.(2.19). Bracken and Melloy [4] used numerical methods to find the most negative eigenvalue $\Delta_{max}(\epsilon)$ of Eq.(5.12). They also looked at how $\Delta_{max}(\epsilon)$ varies for a range of values of the parameter ϵ. We plot their results in Fig.(5.2).

As can be seen in Fig.(5.2), $\Delta_{max}(\epsilon)$ decreases monotonically as ϵ increases. From Eq.(5.14), it is clear that $\Delta_{max}(\epsilon)$ now depends on the parameters $\hbar, m, T$ and the speed of light, c. This is in stark contrast to the non-relativistic case, where the most negative eigenvalue $-c_{bm}$, was a dimensionless quantity [3]. These results may be interpreted in two ways.

Firstly, the amount of backflow decreases if $T \to \hbar/mc^2$, where $\hbar/mc^2$ is an extremely small time of the order of $10^{-21}s$, when relativistic effects become important. Thus one can conclude that these relativistic corrections would be almost impossible to observe in experiment.

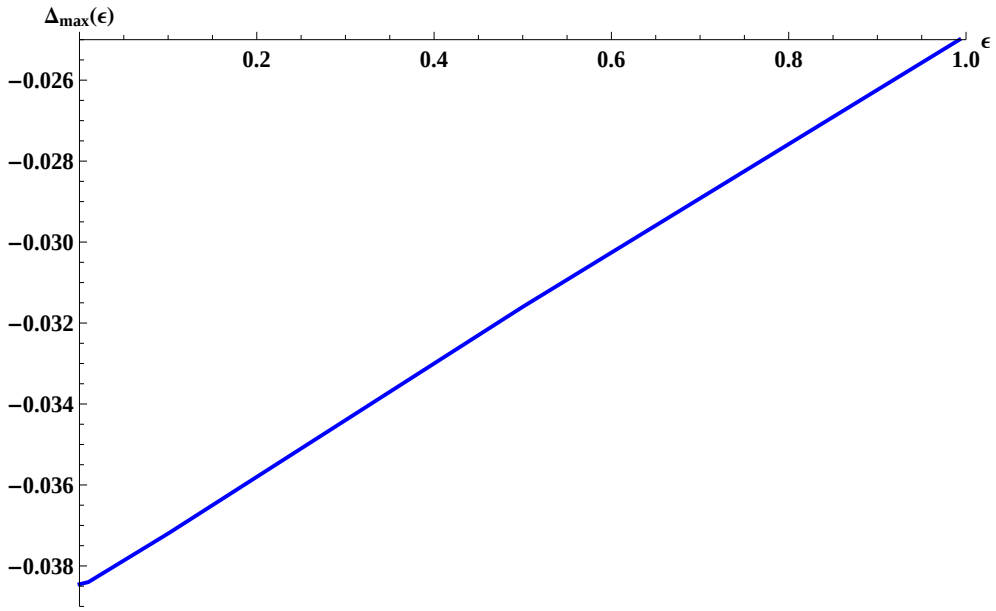

Figure 5.2: Plot of the most negative eigenvalue of Eq.(5.12), $\Delta_{max}(\epsilon)$ as a function of ϵ.

Alternatively, if we choose to fix c, then the most negative value of $\Delta_{max}(\epsilon)$ emerges if $T \to \infty$, $m \to \infty$ or $\hbar \to 0$. In the naive classical limit $\hbar \to 0$, the amount of probability backflow increases. Although this "limit" is an oversimplification, one would expect this clearly non-classical effect to vanish. It is worrying that this is so, however it does coincide with the non-relativistic case, where taking $\hbar \to 0$ does not cause backflow to disappear.

5.4 Backflow Against a Constant Force

If a non-relativistic particle is subject to a constant force $F > 0$ in the positive x-direction, how much probability backflow can occur in opposition to this force over a given time interval $[0, T]$? This question was posed by Bracken and Melloy [6]. Similar to the case of a free particle [3], and Dirac electron [4], the problem becomes one of solving an eigenvalue equation of the form,

$$\frac{1}{\pi}\int_0^\infty \mathrm{d}v\, \frac{\sin[u^2 - v^2 + \alpha(u-v)]}{(u-v)}\phi(v) = \lambda\phi(u) \tag{5.15}$$

where α is a dimensionless parameter defined by

$$\alpha = \frac{FT^{\frac{3}{2}}}{\sqrt{4m\hbar}} \tag{5.16}$$

Note that if $F = 0$ then $\alpha = 0$ and we recover the non-relativistic eigenvalue equation for a free particle, Eq.(2.19). Using numerical methods, the most negative eigenvalue $\Delta_{max}(\alpha)$ of Eq.(5.15) was calculated for a chosen set of values of α. The results are

displayed in Fig.(5.3), and reveal the relationship,

$$\Delta_{max}(\alpha) = -0.039e^{-2\alpha} \tag{5.17}$$

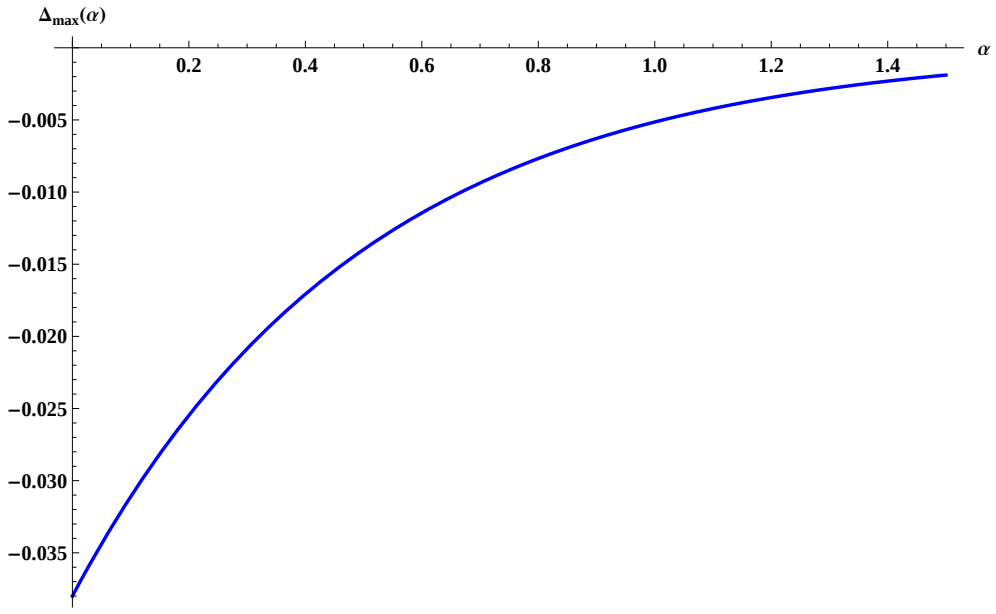

Figure 5.3: Plot of the most negative eigenvalue of Eq.(5.15), $\Delta_{max}(\alpha)$ as a function of α.

As α increases, the value of $\Delta_{max}(\alpha)$ is suppressed by the exponential and decreases. Through Eq.(5.16), it is apparent that $\Delta_{max}(\alpha)$ now depends on the parameters F, m, T and $\hbar$. In the limit $\hbar \to 0$, the backflow effect decreases as one would hope. This is also the case for increasing F or T. What is surprising is that $\Delta_{max}(\alpha)$ actually increases for increasing m.

5.5 Concluding Remarks

The focus of the material presented in this chapter was to highlight different situations where the most negative eigenvalue $-c_{bm}$, which also provides a limit on the maximum possible backflow, becomes dependent on certain physical parameters. Most notably an emphasis was placed on the reappearance of $\hbar$, since letting $\hbar \to 0$ is regarded as restoring the classical limit. Backflow was seen to diminish in both the quasiprojector measurement model and in opposition to a constant force when $\hbar \to 0$. This was not the case for a relativistic particle, however this does agree with the non-relativistic treatment where taking $\hbar \to 0$ does not result in the disappearance of the effect. The process of decoherence provides the best explanation as to why backflow is not evident in classical systems, but by studying these three scenarios a better understanding of the effect has been acquired.

6 Experimental Realisation

6.1 Introduction

It is of great importance that backflow be observed experimentally. This peculiar effect first noted by Allcock [2], emerged in the context of the arrival time problem in quantum mechanics. It has been argued that the time of arrival of a free particle cannot be accurately measured [29], and so one might suspect there to be an inherent difficulty in measuring backflow. It is certainly surprising that no one has yet attempted to do so but exactly what method would be most effective is unclear.

The probability current J is used extensively in the literature on backflow but is generally regarded as being of no operational significance. Attempts have been made to relate the current to measurement [30, 31] and it has even been suggested that J is fundamental in the understanding of scattering phenomena [32]. The most interesting treatment examines special protective measurements of J which do not disturb the wave function [33]. The arguments put forward strongly favour associating physical reality with the quantum state of a single system and these sentiments are reinforced by recent work [34]. If progress is made in determining the current experimentally, the process would naturally lend itself to a measurement of backflow. In this chapter we discuss both direct and indirect methods that may lead to the experimental realisation of backflow. It is felt that for the subject to advance, the effect must be observed.

6.2 Direct Measurement of Backflow

The most direct method of measuring backflow could in principle be done by making position measurements on ensembles of single-particle systems. The flux, Eq.(2.14), can be defined as

$$F(t_1, t_2) = \langle \Pi(t_2) \rangle - \langle \Pi(t_1) \rangle \tag{6.1}$$

which is the difference between two probabilities. If we possessed two identical ensembles, each prepared in the initial state $|\psi\rangle$, then it is possible to deduce the flux. A measurement on the first ensemble to determine if the particle is in $x > 0$ at time t_1, would yield $\langle \Pi(t_1) \rangle$. The same measurement performed on the second ensemble at time t_2, would give $\langle \Pi(t_2) \rangle$. If $\langle \Pi(t_1) \rangle > \langle \Pi(t_2) \rangle$, the flux, Eq.(6.1), is negative and there is backflow.

Yearsley et al [1] suggest that this could be achieved using a weakly interacting Bose-Einstein condensate, since a single measurement on the condensate is effectively a measurement on an ensemble of non-relativistic particles. The main challenge is the preparation of identical initial states consisting of only positive momentum. As we saw earlier in Sec.(4.3), a superposition of Gaussian wavepackets is experimentally viable but does not produce a large amount of backflow. One may ask the question; what state can be prepared experimentally to demonstrate backflow? The answer potentially

is a Schrödinger cat state, and we will discuss this in Sec.(6.4).

Bracken and Melloy [3] propose that a more practicable alternative would be to measure the electric current density, since this is proportional to the probability current, for an electrically charged particle. The initial states of the particles must be prepared with only positive velocity components but these can be of arbitrary size. For each particle a measurement of the electric current density is made at subsequent intervals of time. If one were to observe a current density in direct opposition to the velocity (multiplied by the charge), then this would confirm the presence of backflow. However the feasibility of such a scheme is questionable. One must measure to great accuracy an extremely small amount of current due to a single electric charge moving on the scale of micrometres per microsecond. The delicate nature of such a measurement, and also its reproducibility, suggest it is unlikely that backflow will be observed in this way.

6.3 Complex Potential Model for Arrival Time

The arrival time problem is inextricably linked with the backflow effect. Here, we are concerned with finding the probability that an incoming wavepacket arrives at $x = 0$ during a fixed time interval. There exist many different approaches to this problem [35–39], but in some specific models it is possible to extract the current explicitly from the arrival time probability. For states displaying backflow the current is negative whereas the arrival time probability is non-negative. A noticeable difference between these two quantities will give a clear indication of backflow.

We consider an initial wavepacket localised in $x < 0$ consisting entirely of positive momenta and introduce a complex absorbing potential, $-iV_0\theta(\hat{x})$, of step function form in $x > 0$. (See Ref. [9, 40–42] for other arrival time approaches with a complex potential). The total non-hermitian Hamiltonian is

$$H = H_0 - iV_0\theta(\hat{x}) \tag{6.2}$$

where H_0 is the free Hamiltonian. The probability that the wavepacket is in $x < 0$ and has yet to be absorbed by the complex potential is given by the survival probability $N(\tau)$, defined as

$$N(\tau) = \langle\psi_\tau|\psi_\tau\rangle \tag{6.3}$$

where the state $|\psi\rangle$, evolved for a time τ with the complex Hamiltonian Eq.(6.2), is described by

$$|\psi_\tau\rangle = \exp(-iH_0 - V_0\theta(\hat{x}))\tau|\psi\rangle \tag{6.4}$$

The probability for the wavepacket to cross $x = 0$ in the time interval $[\tau, \tau + d\tau]$ is then the arrival time distribution,

$$\begin{aligned}\mathbf{\Pi}(\tau) &= -\frac{\mathrm{d}N}{\mathrm{d}\tau} \\ &= 2V_0\langle\psi_\tau|\theta(\hat{x})|\psi_\tau\rangle\end{aligned} \tag{6.5}$$

If we differentiate with respect to τ then

$$\frac{\mathrm{d}\mathbf{\Pi}}{\mathrm{d}\tau} = -2V_0\mathbf{\Pi} + 2V_0\langle\psi_\tau|\hat{J}|\psi_\tau\rangle \tag{6.6}$$

where $\hat{J}$ is the current operator, Eq.(2.13). We see that Eq.(6.6) is a differential equation for $\mathbf{\Pi}(\tau)$ and can be solved to give

$$\mathbf{\Pi}(\tau) = 2V_0 \int_{-\infty}^{\tau} \mathrm{d}t\, e^{-2V_0(\tau-t)}\langle\psi_\tau|\hat{J}|\psi_\tau\rangle \tag{6.7}$$

Assuming $\mathbf{\Pi}(\tau) \to 0$ as $\tau \to -\infty$, then Eq.(6.7) is the exact expression for $\mathbf{\Pi}(\tau)$ and shows the explicit dependence on the current operator $\hat{J}$. Although $\hat{J}$ is not a positive operator, Eq.(6.7) is positive by construction. How backflow will affect $\mathbf{\Pi}(\tau)$ is unclear, so it is helpful to only consider the usual weak measurement approximation where V_0 is taken to be small and we may neglect the complex potential term in $|\psi_\tau\rangle$. The arrival time distribution is then

$$\begin{aligned}\mathbf{\Pi}(\tau) &\approx 2V_0 \int_0^{\tau} \mathrm{d}t\, e^{-2V_0(\tau-t)}\langle\psi_t|\hat{J}|\psi_t\rangle \\ &= 2V_0 \int_0^{\tau} \mathrm{d}t\, e^{-2V_0(\tau-t)} J(t)\end{aligned} \tag{6.8}$$

where $|\psi_t\rangle = e^{-iH_0t}|\psi\rangle$. The distribution $\mathbf{\Pi}(\tau)$ is no longer strictly positive because the current may be negative for states that display backflow. Even integration over time does not necessarily ensure the positivity of Eq.(6.8). We only took the limit $V_0 \to 0$ for the complex potential term in $|\psi_\tau\rangle$, but not in the rest of the expression, so the positivity observed in Eq.(6.7) is not preserved. However, for sufficiently small V_0 this is not significant, and $\mathbf{\Pi}(\tau)$ can be regarded as the arrival time distribution measured by a realistic measurement. This in principle can be determined experimentally and by using the process of deconvolution [43, 44], the current (and consequently the flux), can be calculated from Eq.(6.8).

For states that exhibit backflow the flux is negative, whereas the probability for crossing $x = 0$ during the time interval $[t_1, t_2]$, defined as

$$\mathrm{P}(t_1, t_2) = \int_{t_1}^{t_2} \mathrm{d}t\, \mathbf{\Pi}(t) \tag{6.9}$$

is a strictly positive quantity. A comparison of the two values provides a way to potentially observe backflow if there is a significant difference between them.

Note that Eq.(6.8) has the form of the current smeared over a period of time. A region of negative current will counteract and essentially cancel out a region of positive current in the measured probability $\mathbf{\Pi}(\tau)$. It is possible then, that backflow causes a time delay between the arrival of the wavepacket at $x = 0$ and its detection in a measuring device.

Already it has been shown that for an idealised particle detection model that uses a complex potential, the backflow effect has startling implications when considering the concept of perfect absorption at the origin [10]. During an interval of backflow it is

possible for a perfect absorber to emit probability. This is to compensate for the small amount of probability that has already entered the detector volume before the period of backflow, but has not been absorbed. The effect is only temporary however and no particles are permanently reflected if we are to assume the detector behaves as a perfect absorber. We also mention that at asymptotic distances from the source or interaction region, the effect of backflow is negligible [9].

Yearsley et al [1] looked at how probability backflow is affected by a time-smeared current. Their plot of the current for the backflow maximising state, compared with the time-smeared current Eq.(6.8) for two values of V_0, can be seen in Fig.(6.1).

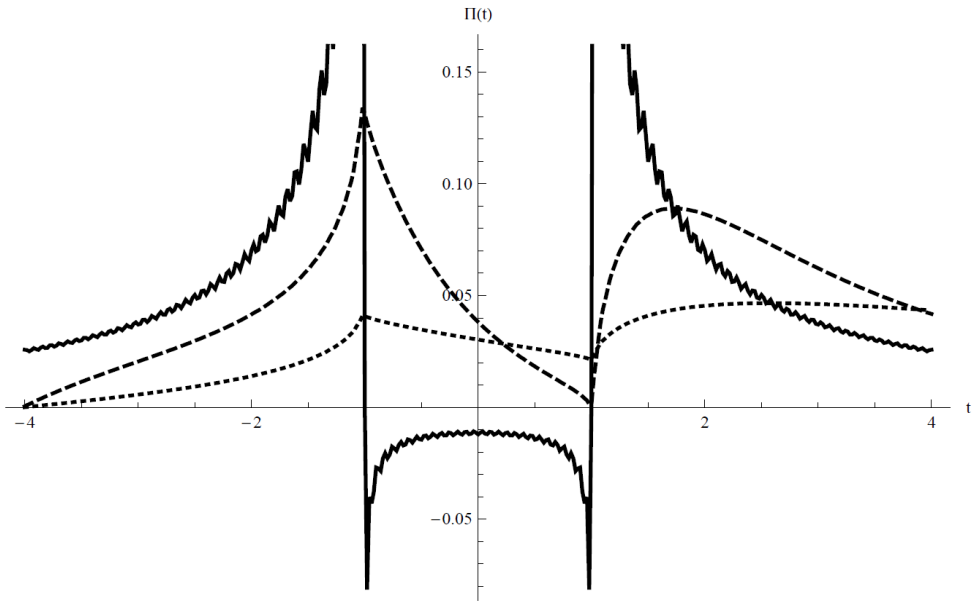

Figure 6.1: A comparison of the backflow maximising current (solid line) with the time-smeared current Eq.(6.8) for $V_0 = 0.5$ (dashed line) and $V_0 = 0.1$ (dotted line) [1].

There are no longer any periods of negativity due to the time-smearing of the current. The behaviour at $t = \pm 1$ is now characterized by discontinuous changes in the derivative of the time-smeared current rather than the distinctive singularity structure. These discontinuities are possible signatures (in the measured probabilities) of the backflow effect.

6.4 Schrödinger Cat State

A Schrödinger cat state is a superposition of two maximally different quantum states. For our purposes we are interested in a superposition of spatially separated coherent states described by the wave function,

$$|\psi_{cat}\rangle = a|\alpha\rangle + b|-\alpha\rangle \qquad a, b \in \mathbb{C} \tag{6.10}$$

where $|\alpha\rangle$ is a coherent state which is specified by a single complex number α. Coher-

ent states are minimum uncertainty states, and in the position representation can be expressed as

$$\psi_\alpha(x) = \langle x|\alpha\rangle = A \exp\left(-\left(\sqrt{\frac{m\omega}{2\hbar}}x + \alpha\right)^2\right) \tag{6.11}$$

where A is a normalisation constant given by,

$$A = \left(\frac{m\omega}{\pi\hbar}\right)^{\frac{1}{4}} \exp\left(\frac{1}{2}\alpha(\alpha - \alpha^*)\right) \tag{6.12}$$

The time dependence of the coherent state is obtained by acting with the time evolution operator $U(t) = \exp(-iHt/\hbar)$, and it follows that

$$U(t)|\alpha\rangle = |\alpha(t)\rangle = e^{-\frac{i}{2}\omega t}|\alpha e^{-i\omega t}\rangle \tag{6.13}$$

A coherent state remains coherent as time evolves. The time dependent wave function of the cat state, expressed in the position representation, is now

$$\psi_{cat}(x,t) = a\psi_\alpha(x,t) + b\psi_{-\alpha}(x,t) \tag{6.14}$$

The state $\psi_{cat}(x,t)$ is a superposition with arbitrary weights of two coherent states symmetrically placed with respect to the origin. The preparation of cat states is challenging as they are very susceptible to decoherence, but states of this form have been realised experimentally [45, 46]. Most notably, a cat state of the harmonic oscillator has been created by preparing a superposition of two coherent state wavepackets of a single trapped ion in one dimension [47, 48]. This approach enables the harmonic motion of the trapped ion to be controlled to a high degree of accuracy, and because of the time evolution of a coherent state, the separation of the superposition is preserved.

It is the motion of the ion in the trap that may lead to the observation of backflow. For the effect to occur, one of the two components of the wave function must overtake and interfere with the other. However, $\psi_{cat}(x,t)$ is a symmetric state and will not display backflow. It is experimentally possible though, to manipulate $\psi_{cat}(x,t)$ so that it is no longer symmetric. This is achieved by applying a single pulse of an additional dc electric field to displace the ion from the trap centre. The cat state will then be of the form,

$$|\psi_{cat}\rangle = a|\alpha\rangle + b|\beta\rangle \tag{6.15}$$

where α and β are real and non-negative, and this state will produce backflow. A plot of the current Eq.(2.2), at $x = 0$, is shown in Fig.(6.2) and Fig.(6.3) for the following parameters,

$$a = \sqrt{\frac{3}{4}}, \quad b = \sqrt{\frac{1}{4}}, \quad \alpha = 1.5, \quad \beta = 9, \quad \omega = 1 \tag{6.16}$$

with $\hbar = 1$ and $m = 1$. The parameters chosen were to illustrate the negativity of the current and in principle are experimentally viable.

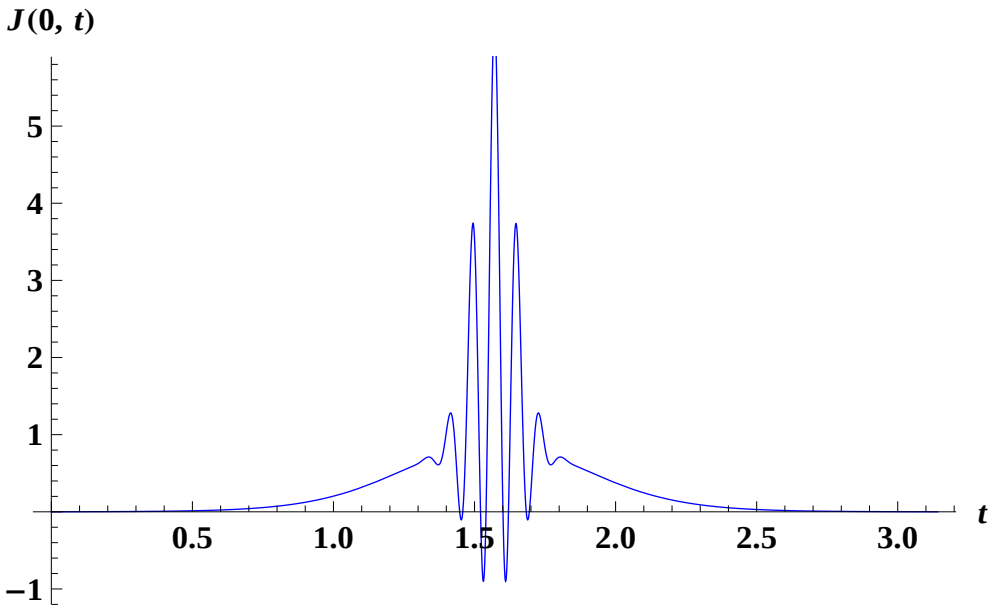

Figure 6.2: Plot of $J(0,t)$ for a wave function consisting of a superposition of two coherent states, with the parameters specified in Eq.(6.16).

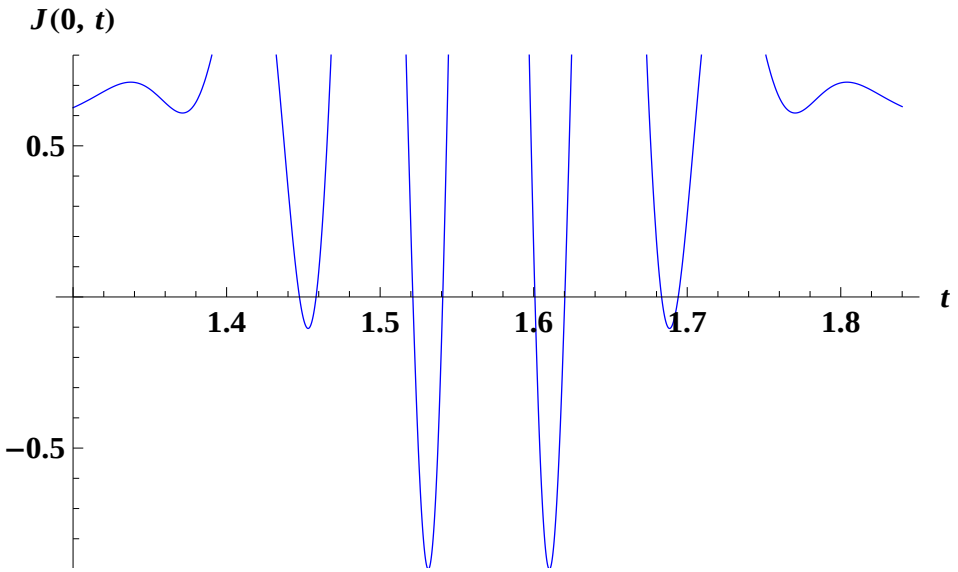

Figure 6.3: Close up of Fig.(6.2). The current is clearly seen to be negative at several times.

The current has two strong negative peaks for the time interval $[0,\pi]$, best seen in Fig.(6.3). A plot of the probability for remaining in $x < 0$ is shown in Fig.(6.4). Like the example of a superposition of two Gaussian wavepackets in Sec.(4.3), backflow occurs in several disjoint time intervals. The value of the flux during the largest period of backflow is calculated to be,

$$F \approx -0.0116 \tag{6.17}$$

which is around 30% of the theoretical maximum. The backflowing fraction of the x-axis has the value,

$$P_{back} = 0.1404 \tag{6.18}$$

Both the negative flux and P_{back} are larger for the cat state when compared with a superposition of two Gaussians. This is encouraging for the experimental observation of the effect, even though the amount of backflow is still significantly less than the theoretical maximum.

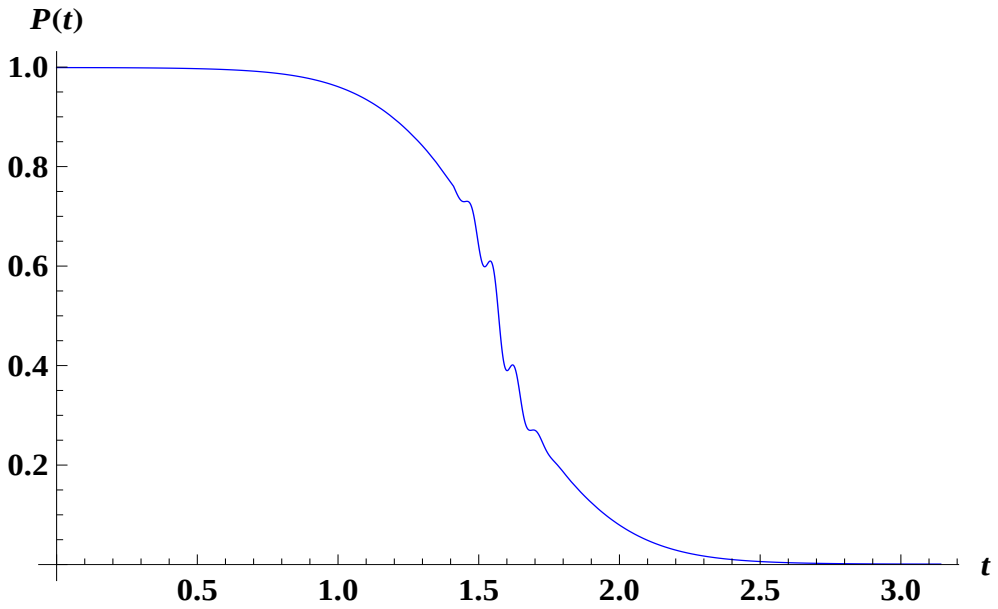

Figure 6.4: Plot of the probability for remaining in $x < 0$ as a function of time for the Schrödinger cat state.

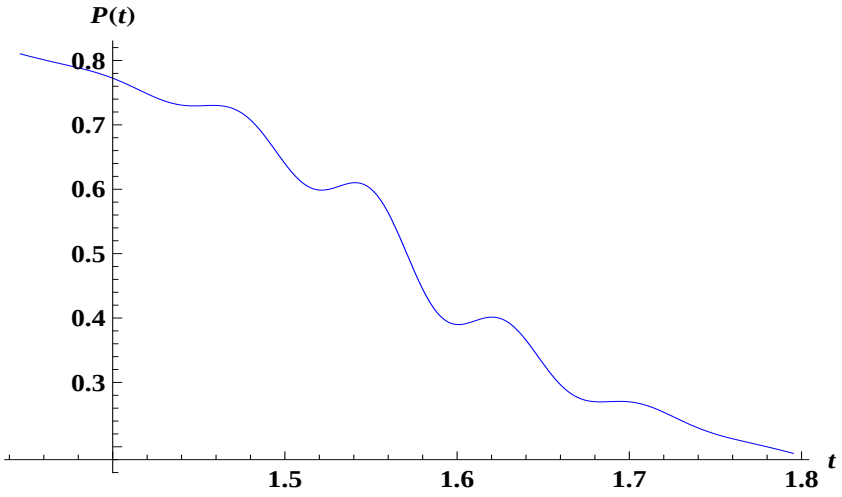

Figure 6.5: Close up of Fig.(6.4). The probability is clearly seen to increase.

It is possible to increase the amount of backflow by modifying the values of α and β. However, a Schrödinger cat state has support on both positive and negative momentum therefore it is necessary to confirm the occurrence of backflow is not the result of any negative momenta in the wavepacket. A series of plots of the momentum distribution of the cat state for various times during the interval, $0 \leq t \leq \pi$, is shown in Fig.(6.6). At $t = 0.8$, the cat state is almost entirely composed of positive momentum. During a period of backflow ($t = 1.6$), the momentum distribution of $|\alpha\rangle$ is centred around $p \approx 2.1$, and an estimate of the fraction of the wavepacket located in $p < 0$ shows approximately 0.1% of the wavepacket consists of negative momentum. This is negligible and demonstrates that the negativity of the flux is due to the backflow effect.

Note that the Wigner function of a cat state displays Gaussian like probabilities localised in two different regions of phase space plus a strong interference term which takes negative values [49]. As discussed in Sec.(2.1), it is this negativity that is a necessary condition for the negativity of the flux.

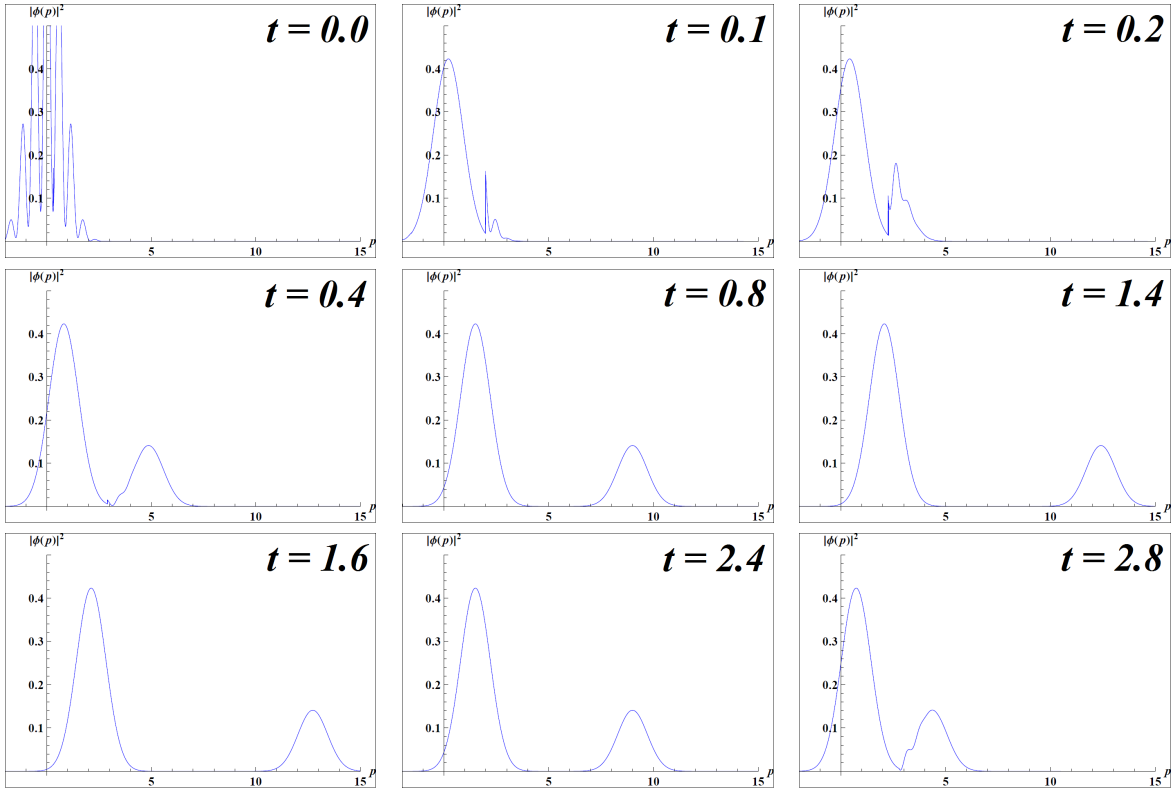

Figure 6.6: Plot of the momentum distribution of the Schrödinger cat state for various times during the interval, $0 \leq t \leq \pi$.

A method similar to that described in Sec.(6.2) could be used to detect backflow. Position measurements on the ion must be performed with a temporal resolution that is less than the period of the trap. Shining a laser on the ion at resonance will emit a large number of photons that would indicate its position, however there are concerns with this approach. A laser can impart more momentum to the ion which may disturb

the harmonic motion and more importantly, any measurement that reveals the position of the ion to within the uncertainty of its wave function will destroy the quantum state. An indirect method could prove more fruitful, but precisely what this might entail is unclear. It is important that any interaction with the state does not lead to decoherence. The field of ion trap manipulation is now well established and one suspects that the techniques required to detect backflow already exist. All that is needed is an experimentalist with the expertise to finally realise this quantum effect.

The material presented in this section is in its infancy but does show promise. Further work must establish the optimum values for α and β to maximise backflow but also confirm that negative momentum is not responsible. It could be that experimental limitations mean only a small range of values are accessible to α and β.

7 Summary and Further Work

7.1 Summary

The aim of this report was to provide a detailed account of the quantum backflow effect. In Chapter 2 it was shown that when the current at the origin $J(0,t) < 0$, the probability of remaining in $x < 0$ can increase with time. To understand this behaviour we developed the relationship between the Wigner function and the current. Negative values of the Wigner function arise from interference between different portions of the wavepacket and it is this negativity that is a necessary condition for the negativity of the current. The backflow eigenvalue equation was set up and solved numerically to find the most negative eigenvalue of the flux operator. This led to the appearance of the dimensionless quantity c_{bm}. The backflow maximising state was numerically computed and a plot of the resulting wave function shown in momentum and configuration space. A plot of the resulting current revealed a distinctive singularity structure at $t = \pm 1$. The flux operator was shown to be linear bounded, self-adjoint and non-compact.

The spatial extent of backflow was explored in Chapter 3. A quantum inequality for the current demonstrated that backflow is limited in space. The backflowing fraction of the x-axis was characterised by the backflow probability P_{back}, which approaches its maximal value of $1/2$ when the component momenta in the wavepacket are strongly correlated. The connection between backflow and superoscillations was explored. There appeared to be striking similarities between the time evolution of fast superoscillations and strong backflow.

In Chapter 4 the example of a superposition of two plane waves was used to illustrate the backflow effect. This demonstrated that negative values of the current can be understood as an interference effect. It was also shown that the width of a region of backflow decreases as the wavenumber $k(x)$ becomes more negative. The current and the flux were computed for a superposition of two Gaussian wavepackets. Although experimentally realisable, this state displays only 16% of the maximum possible backflow, a very small amount. A normalisable state significant in the development of the subject was studied and shown to display 11% of the theoretical maximum backflow. A candidate analytic expression for the backflow maximising state was presented which appeared to follow closely the numerical solution of Penz et al [8]. However a plot of the current failed to match the distinctive singularity structure at $t = \pm 1$ which is perhaps an important characteristic of the backflow maximising state.

In Chapter 5 we examined three different scenarios where the most negative eigenvalue $-c_{bm}$, becomes dependent on certain physical parameters. The more realistic measurement model of quasiprojectors restored the naive classical limit, and backflow was seen to diminish when $\hbar \to 0$. In the relativistic case for particles governed by the Dirac equation, the maximum amount of backflow Δ_{max} depends on the dimensionless combination $mc^2T/\hbar$. Backflow can occur in opposition to a constant force but the effect gets smaller when the size of the force is increased.

The experimental realisation of backflow was discussed in Chapter 6. A direct method to measure backflow could in principle be done by making position measurements on ensembles of single-particle systems. A complex potential model often used in the arrival time problem could lead to the observation of backflow. If the arrival time distribution $\mathbf{\Pi}(\tau)$ can be determined, it is possible to extract the current by deconvolution and then from this calculate the flux. Backflow was also noted to have certain implications for the concept of perfect absorption. A Schrödinger cat state which is experimentally realisable was shown to exhibit backflow. The scheme presented shows promise but requires further work.

7.2 Open Questions and Further Work

Time Scale of Backflow

It is always possible to find a state which exhibits backflow for an arbitrarily long period of time but this does not tell us about the 'natural' time scale for which this effect takes place. The relationship established in Eq.(2.24) demonstrated that the current can be arbitrarily negative if only for a sufficiently short time. Does the magnitude of the negative current dictate the time scale on which backflow occurs? If not, is it some property of the type of state that determines the duration of a period of backflow? These questions reaffirm the need for experimental observation of the effect. If a successful method to determine the flux was found, the amount of backflow for different states could be measured and compared not only with each other, but also their own theoretical maximum values. This would establish whether or not a state will always display the same amount of backflow.

Analytic Calculation of the Eigenvalue Equation

Penz et al [8] questioned whether there really is a backflow eigenvalue, in the strict mathematical sense, that $-c_{bm}$ is an approximation to. The analytic calculation of $-c_{bm}$ and the analytic form of the backflow maximising state will no doubt be found if there is a continued effort to do so. This optimism is confirmed by the progress made in the recent work of Yearsley et al [1], who also speculate that perhaps the non-commutativity of the operators $\theta(\hat{p})$ and $\theta(-\hat{x})$ will lead to an analytic calculation of the quantity $-c_{bm}$.

Eigenstates of the Flux Operator

The backflow maximising state is an eigenstate of the flux operator $\hat{F}(t_1, t_2)$ with eigenvalue $-c_{bm}$. Here is a quantum state that describes a non-relativistic free particle which displays the maximum amount of backflow. How does one interpret the other eigenstates of the flux operator though? Specifically what does it mean for the eigenstate which has eigenvalue $+1$? A plot of this state in momentum space is shown in Fig.(7.1). It has a slightly different form to the backflow maximising state Fig.(2.1). The behaviour at large u is unclear because a momentum cut-off must be introduced to solve the backflow eigenvalue equation numerically. It would appear that the state tends towards some asymptotic form, however further investigation is needed.

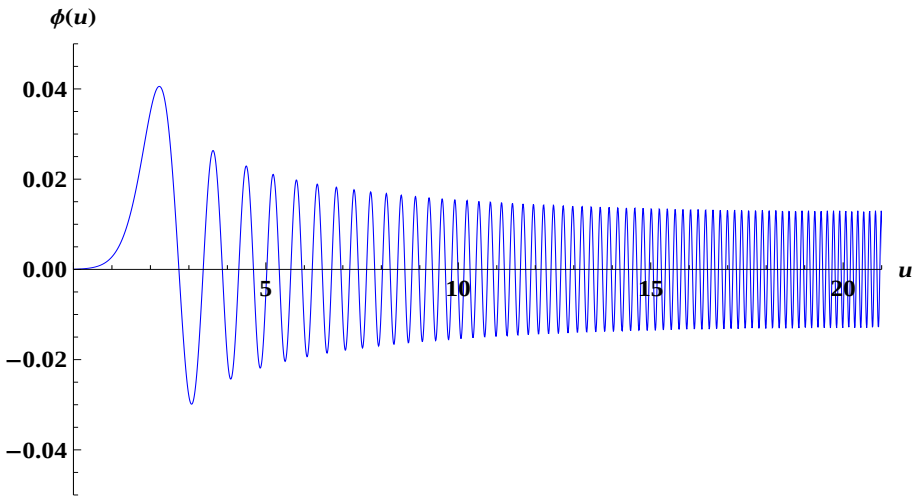

Figure 7.1: Plot of the eigenstate of the flux operator with eigenvalue +1 in momentum space.

A plot of the current at the origin is shown in Fig.(7.2). There are large positive values of J, but also short periods of negativity indicating that this eigenstate exhibits backflow too. Since the flux of this state is +1, the probability for remaining in $x < 0$ rapidly decreases with all the probability crossing $x = 0$ in the time interval $[-1, 1]$. This suggests the eigenstate consists of a wavepacket with high velocity which crosses the origin in its entirety during $[-1, 1]$.

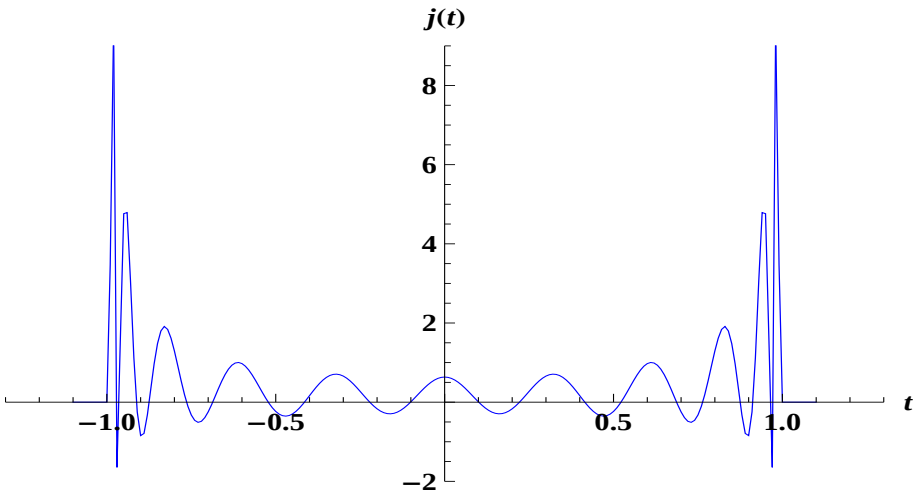

Figure 7.2: Plot of $J(0, t)$ for the eigenstate of the flux operator with eigenvalue +1.

It would be of great interest to look in more detail at the other eigenstates of the flux operator. Not only would it help our interpretation of these states but it could well provide clues to the analytic form of the backflow maximising state.

References

[1] J.M.Yearsley, J.J.Halliwell, R.Hartshorn, and A.Whitby, e-print arXiv:1202.1783v4 (2012).

[2] G.R.Allcock, Ann.Phys. **53**, 253 (1969); **53**, 286 (1969); **53**, 311 (1969).

[3] A.J.Bracken and G.F.Melloy, J.Phys.A **27**, 2197 (1994).

[4] A.J.Bracken and G.F.Melloy, Found.Phys. **28**, 505 (1998).

[5] M.V.Berry, J.Phys.A **43**, 415302 (2010).

[6] A.J.Bracken and G.F.Melloy, Ann.Phys.(Leipzig) **7**, 726 (1998).

[7] S.P.Eveson, C.J.Fewster, and R.Verch, Ann.Inst. H.Poincaré **6**, 1 (2005).

[8] M.Penz, G.Grübl, S.Kreidl, and P.Wagner, J.Phys.A **39**, 423 (2006).

[9] J.G.Muga, S.Brouard, and D.Macías, Ann.Phys. **240**, 351 (1995).

[10] J.G.Muga, J.P.Palao, and C.R.Leavens, Phys.Lett.A **253**, 21 (1999).

[11] M.Ruggenthaler, G.Grübl, and S.Kreidl, J.Phys.A **38**, 8445 (2005).

[12] P.Strange, Eur.J.Phys. **33**, 1147 (2012).

[13] J.M.Yearsley, Phys.Rev.A **82**, 012116 (2010).

[14] J.J.Halliwell and J.M.Yearsley, Phys.Rev.A **79**, 062101 (2009).

[15] J.M.Yearsley, Aspects of Time in Quantum Theory, Imperial College PhD Thesis available as quant-ph/1110.5790 (2011).

[16] J.J.Halliwell and J.M.Yearsley, Phys.Lett.A **374**, 154 (2009).

[17] B.Misra and E.C.G.Sudarshan, J.Math.Phys. **18**, 756 (1977).

[18] N.Balasz and B.K.Jennings, Phys.Rep. **104**, 347 (1984).
M.Hillery, R.F.O'Connell, M.O.Scully, and E.P.Wigner, Phys.Rep. **106**, 121 (1984).

[19] R.P.Feynman, Quantum Implications: Essays in Honour of David Bohm, B.J.Hiley and F.D.Peat (eds) p. 235 (Routledge and Kegan Paul, 1987).

[20] L.Diósi and C.Kiefer, J.Phys.A **35**, 2675 (2002).
P.J.Dodd and J.J.Halliwell, Phys.Rev.A **69**, 052105 (2004).

[21] N.N.Bogolubov, A.A.Logunov, A.I.Oksak, and I.T.Todorov, General Principles of Quantum Field Theory p. 100 (Kluwer Academic Publishers, Dordrecht, 1990).

[22] Y.Aharonov, J.Anadan, S.Popescu, and L.Vaidman, Phys.Rev.Lett. **64**, 2965 (1990).

[23] Y.Aharonov, D.Z.Albert, and L.Vaidman, Phys.Rev.Lett **60**, 1351 (1988).

[24] M.V.Berry and P.Shukla, J.Phys.A **43**, 354024 (2010).

[25] Y.Aharonov, F.Colombo, I.Sabadini, D.C.Struppa, and J.Tollaksen, J.Phys.A **44**, 365304 (2011).

[26] M.V.Berry and S.Popescu, J.Phys.A **39**, 6965 (2006).

[27] J.H.Eberly, N.B.Narozhny, and J.J.Sanchez-Mondragon, Phys.Rev.Lett. **44**, 1323 (1980).

[28] P.J.S.G.Ferreira and A.Kempf, IEEE Trans.Signal Processing **54**, 3732 (2006).

[29] Y.Aharonov, J.Oppenheim, S.Popescu, B.Reznik, and W.G.Unruh, Phys.Rev.A **57**, 4130 (1998).

[30] W.Gale, E.Guth, and G.T.Trammell, Phys.Rev. **165**, 1434 (1968).

[31] D.J.Mason, M.F.Borunda, and E.J.Heller, cond-mat/1205.0291 (2012).

[32] M.Daumer, D.Dürr, S.Goldstein, and N.Zanghi, J.Stat.Phys. **88**, 967 (1997).

[33] Y.Aharonov and L.Vaidman, Phys.Lett.A **178**, 38 (1993).

[34] M.F.Pusey, J.Barrett, and T.Rudolph, Nature Physics **8**, 476 (2012).

[35] N.Grot, C.Rovelli, and R.S.Tate, Phys.Rev.A **54**, 4676 (1996).

[36] V.Delgado and J.G.Muga, Phys.Rev.A **56**, 3425 (1997).

[37] J.G.Muga and C.R.Leavens, Phys.Rep. **338**, 353 (2000).

[38] J.G.Muga, R.Sala Mayato, and I.L.Egusquiza (eds), Time In Quantum Mechanics (Springer, Berlin, 2002).

[39] J.M.Yearsley, D.A.Downs, J.J.Halliwell, and A.K.Hashagen, Phys.Rev.A **84**, 022109 (2011).

[40] J.J.Halliwell, Prog.Th.Phys. **102**, 707 (1999).

[41] J.Echanobe, A.del Campo, and J.G.Muga, Phys.Rev.A **77**, 032112 (2008).

[42] J.J.Halliwell, Phys.Rev.A **77**, 062103 (2008).

[43] J.A.Damborenea, I.L.Egusquiza, G.C.Hegerfeld, and J.G.Muga, Phys.Rev.A **66**, 052104 (2002).

[44] G.C.Hegerfeld, D.Seidel, and J.G.Muga, Phys.Rev.A **68**, 022111 (2003).

[45] D.Leibfried et al, Nature **438**, 639 (2005).

[46] X.C.Yao et al, Nature Photon. **6**, 225 (2012).

[47] C.Monroe, D.M.Meekhof, B.E.King, and D.J.Wineland, Science **272**, 1131 (1996).

[48] C.Monroe, D.M.Meekhof, B.E.King, D.Liebfried, W.M.Itano, and D.J.Wineland, Acc.Chem.Res. **29**, 585 (1996).

[49] E.Colavita and S.Hacyan, Rev.Mex.Fis. **49**, 45 (2003).